Characterization of a microscope objective for a second generation Dysprosium quantum gas experiment

Bachelor thesis
by
Magnus Benke

submitted to the University of Stuttgart

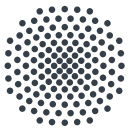

Universität Stuttgart

Prüfer: Tilman Pfau
5. Physikalisches Institut,
Universität Stuttgart,
23. Oktober 2020

Abstract

In this thesis, the performance of a custom microscope objective for a new experiment with ultracold Dysprosium atoms, at the 5th Physical Institute at the University of Stuttgart is characterized. By simulating the objective in an optical system that follows the configuration of the planned imaging setup, the sensitivity of the system to misalignments in all individual components are investigated. By analyzing the point-spread function, the limits at which the system is no longer diffraction limited are determined, and the ability to compensate aberrations from a misaligned objective with a deliberate displacement of a second focusing lens is demonstrated. A test setup with the required precise translational and rotational control of the optical elements for diffraction-limited imaging is built, and initial images with a 1 µm pinhole and a 200 nm aperture scanning near-field optical microscope-fiber tip are presented. With further optimization of this test setup, it is possible to obtain images that confirm the microscope objective to be diffraction limited, as designed.

Zusammenfassung

In dieser Arbeit wird das Objektiv eines Mikroskops für das neue Experiment mit ultrakalten Dysprosium Atomen am 5. Physikalischen Institut der Universität Stuttgart charakterisiert. Mit Simulationen des Objektives in einer vergleichbaren Konfiguration wie im geplanten Aufbau wird die Sensitivität des Systems gegenüber Fehlausrichtungen in allen individuellen Komponenten untersucht. Durch Auswerten der Punktspreizfunktion wird die Auflösungsgrenze des Systems ermittelt und gezeigt, dass durch gezieltes Verstellen einer zweiten Sammellinse eine Fehlausrichtung des Objektives kompensiert werden kann. Ein Testaufbau mit den benötigten präzisen Verstellmöglichkeiten zum Erreichen der Auflösungsgrenze wird beschrieben und erste Bilder einer 1 µm großen Iris und dem 200 nm großen Faserendes eines optischen Rasternahfeldmikroskops werden gezeigt. Mit weiteren Optimierungen des Aufbaus ist es möglich, Objekte an der Auflösungsgrenze des Objektives abzubilden

Ehrenwörliche Erklärung

Hiermit versichere ich,

- dass ich meine Arbeit selbständig verfasst habe,
- dass ich keine anderen als die angegebenen Quellen benutzt und alle wörtlich oder sinngemäß aus anderen Werken übernommenen Aussagen als solche gekennzeichnet habe,
- dass ich die eingereichte Arbeit weder vollständig noch in wesentlichen Teilen als Gegenstand eines anderen Prüfungsverfahrens verwendet habe, und
- dass das elektronische Exemplar mit den anderen Exemplaren übereinstimmt.

Stuttgart, 23. Oktober 2020 Magnus Benke

Contents

1 Introduction

First predicted by A. Einstein and S. Bose in 1924 [1], the Bose-Einstein condensate (BEC) was first observed in 1995 by E. Cornell and C. Wieman using Rubidium atoms. Realizing this new state of matter resulted in the awarding of the Nobel Prize in 2001 [2]. As of today, many other elements have been successfully condensed to a BEC, opening up the possibility to study ultracold gases and their interactions and as well discover new states of matter. In 2005 T. Pfau et. al reported the successful production of a BEC using Chromium atoms [3], not dominated by the short range contact-interactions as earlier BECs created before. With this, the dipolar effects in ultracold quantum gases can be studied. Since then, Chromium has been replaced with Dysprosium, because of its considerably higher magnetic moment. This has lead to the observation of dilute quantum droplets [4] and the supersolid state of matter [5]. To further enable more new discoveries, a second generation of the experimental setup is currently being built that will also takes advantage of the large magnetic dipole moment of Dysprosium. With this new setup, it will be possible to image BECs that contain a larger number of atoms, compared to the current experiment, with a higher resolution. As a result, it is possible to investigate phenomena such as the Higgs mode in a dipolar supersolid [6], vortices in a superfluid dipolar quantum gas [7], and the arrangement of droplets in two-dimensional configurations [8, 9].
In the new setup, a custom microscope objective is used to image the ultracold Dysprosium atom cloud and also provide the ability to imprint time-averaged potentials on the cloud. For imaging, light of the wavelength $\lambda_1 = 421\,\text{nm}$, and for imprinting potentials, the wavelength $\lambda_2 = 532\,\text{nm}$ is used. To not affect the potential or the image of the atoms, the objective should be diffraction limited.
Motivated by the work from C. Robens [10] and F. Kleissler [11], who used a scanning near-field optical microscopy(SNOM)-fiber tip for the characterization of a high-numerical aperture objective lens, the goal for this thesis is to characterize the objective for the new setup. The objective must be capable of imaging small structures in a diffraction limited system for both wavelengths with precise control to minimize aberrations. To confirm that and also determine the optimal positions and ranges for all optical elements for a diffraction-limited system, a test setup of the imaging system that incorporates the microscope objective is designed and built. In this setup, the limits of the objective can be reached and a statement of whether it is suitable fo use in the new experiment can be given.
For that purpose first the theory for an optical system using Gaussian optics is described (Sec. 2.1). This leads into the definition of the Airy disk (Sec. 2.2) and the point-spread function (Sec. 2.3). All optical components are not perfect and therefore will cause aberrations, the most likely aberrations to occur are discussed in Sec. 2.5. Every component used in the test and how its relative positions can be controlled is described in detail in Sec. 3, as well as the procedure of building the test setup (Sec. 3.8) is included there. Following this, simulations for decentering, tilting and movements along the optical axis for all relevant parts are analyzed and discussed (Sec. 4). All simulations are done with λ_1, the results can also be used to estimate the values for λ_2. First images taken with the test setup are part of Sec. 5. Discussed are the shapes of a $2\,\mu\text{m}$ fiber, a $1\,\mu\text{m}$ pinhole and the SNOM-fiber with an aperture of $200\,\text{nm}$.

2 Theory of optical imaging

In this section the basic Gaussian optics is outlined and a mathematical approach for the Airy disc and the point spread function is given. Also optical aberrations that change the spot size and the Airy disk radius are discussed.
A diffraction-limited system is a system with a resolution limited only by the optical restriction of diffraction. This resolution limit can be characterized with the Abbe diffraction limit [12]

$$d = \frac{\lambda}{2NA}, \tag{1}$$

where λ is the wavelength of the light and NA the numerical aperture. The NA characterizes the angle range, in which an optical component can focus down a beam. The Abbe limit gives the minimal distance d that two point sources can still be resolved.
A more general approach to the diffraction limit can be found in Maznev and Wright [13]:

> The smallest period of the in-plane spatial Fourier components of the energy density distribution in the image plane cannot be less than $\lambda/2$, where λ is the wavelength in the medium (or 'effective medium' for a metamaterial)

And:

> More than 50% of the total energy cannot be focused into a spot smaller than $\sim [n\lambda/2NA]$[1].

The first definition is similar to the Abbe limit. They also state that the second definition is a more practical for an actual measurement, because the spot size containing 50% of the total amount of energy is more relevant and easier to measure in experimental physics. For example the airy disk contains 50% of the total energy in a spot with radius $0.535\lambda/N$. The Airy disk is the description for an image pattern of a focused beam that is diffraction limited.
All three provided definitions show that the diffraction limit is only dependent on the wavelength and numerical aperture, so the optical limitation of the diffraction. In reverse, that means a system is not diffraction limited when the beam shape and the its size are larger than this limit.

2.1 Gaussian optics

Laser beams typically are Gaussian. So Gaussian optics can be used to describe the propagation of the beam. Like all other electromagnetic waves it is a direct consequence from the Maxwell relations and the wave equation [12]

$$\nabla^2 E = \frac{1}{c^2}\frac{\partial^2 E}{\partial t^2}, \tag{2}$$

where c is the speed of light in vacuum. The scalar function $E = E(\mathbf{x},t)$ is dependent on the three-dimensional space coordinates $\mathbf{x} = \{x,y,z)\}$ and the time t. Assuming the angle between optical axis and the propagating beam is small, such that the amplitude will only change by small amounts, the tangent of this angle can be approximated as linear. With this paraxial approximation one possible solution for eq. 2 is

$$E(\rho,z) = E_0 \frac{w_0}{w(z)} \mathrm{e}^{(-\rho/w(z))^2} \mathrm{e}^{ik\frac{\rho^2}{2R(z)}} \mathrm{e}^{i(kz-\eta(z))}, \tag{3}$$

where E_0 is the amplitude, $w(z)$ is the radius, w_0 is the minimal radius or the beam waist, $R(z)$ the radius of curvature and $\eta(z)$ is the Gouy-phase. The transversal coordinate

[1] Changed by the author to match the here used definition of the numerical aperture

$\rho = \sqrt{x^2 + y^2}$ is the distance from the axis z of propagation direction [14]. The radius of the beam is defined by

$$w(z) = w_0 \sqrt{1 + \left(\frac{z}{z_\mathrm{R}}\right)^2}. \tag{4}$$

That means a Gaussian beam has a diameter that is dependent on the distance with a minimum at $z = 0$. The Rayleigh length z_R can be defined by the waist

$$w_0^2 = \frac{\lambda z_\mathrm{R}}{\pi} \tag{5}$$

such that the Rayleigh length describes the point where $w(z_R) = \sqrt{2} w_0$. With that the radius of the beam at all distances is well-defined by the wavelength λ and the waist w_0. The region $-z_\mathrm{R} < z < z_\mathrm{R}$ is called Rayleigh zone and is described with the confocal parameter $b = 2z_\mathrm{R}$.
The radius of curvature for the wavefront is also defined by the Rayleigh length with

$$R(z) = z \left(1 + \left(\frac{z_\mathrm{R}}{z}\right)^2\right). \tag{6}$$

For $|z| << z_\mathrm{R}$ (near field) the radius of curvature is decreasing from infinity at $z = 0$ to a minimal curvature radius $R(z_\mathrm{R}) = 2z_\mathrm{R}$ at the Rayleigh length z_R. In the far field ($|z| >> z_\mathrm{R}$) it is $R(z) \sim z$. The divergence $\Theta_\mathrm{div} = w_0/z_\mathrm{R}$ is the linear approximation for the Gaussian beam in the far field.
The Gouy-phase describes the difference of the phase shift through the focus to a plane wave:

$$\eta(z) = \arctan\left(\frac{z}{z_\mathrm{R}}\right). \tag{7}$$

All parameters with a detailed explanation can be found in [15].
The intensity distribution in the (x,y)-plane is given by

$$I(\rho,z) = \frac{c\varepsilon_0}{2} E E^\star = \frac{c\varepsilon_0}{2} |E_0|^2 \left(\frac{w_0}{w(z)}\right)^2 \mathrm{e}^{-2\left(\frac{\rho}{w(z)}\right)^2}, \tag{8}$$

with the vacuum permittivity ϵ_0. For $z = z_\mathrm{R}$ the intensity maximum is half the maximal intensity at the origin of z, so

$$I(\rho, z = z_\mathrm{R}) = \frac{1}{2} I(\rho, z = 0).$$

2.2 Airy disk

Here only a short introduction in diffraction theory is given. A detailed derivation of the Airy disk and the point spread function can be found in [16] or as a summary in [17], on which the following derivation is oriented at.
As a fundamental principle, the Huygens law will cause diffraction patterns when a light wave will pass an aperture. For a monochromatic light wave $\mathbf{E}(\mathbf{r},t) = \mathbf{E}(\mathbf{r}) \exp\{-i\omega t\}$, which can be assumed for the experiment in this thesis, eq. 2 can be written as the Helmholtz equation

$$\left(\nabla^2 + k^2\right) \mathbf{E}(\mathbf{r}) = 0. \tag{9}$$

With a now three-dimensional coordinate, expressed with P in the position space, and a complex amplitude the monochromatic wave $\mathbf{E}(\mathbf{P},t) = \mathbf{E}(\mathbf{P}) \exp\{-i\omega t\}$ can be calculated with

$$\mathbf{E}(\mathbf{P}_0) = \frac{1}{4\pi} \iint\limits_S \left(\frac{\partial \mathbf{E}(\mathbf{P})}{\partial n} \mathbf{G}(\mathbf{P}) - \mathbf{E}(\mathbf{P}) \frac{\partial \mathbf{G}(\mathbf{P})}{\partial n} \right) dS, \tag{10}$$

where P_0 defines an arbitrary point where the diffraction is observed. Around this point a closed surface S and a Green's function $\mathbf{G}$, representing the outgoing spherical wave, are defined. The inward normal unit vector $\mathbf{n}$ is orthogonal to S. For the spherical wave at a point $\mathbf{P}_1$ on the surface S a point source at $\mathbf{P}_2$ is assumed, so $\mathbf{E}(\mathbf{P}_1) = A\frac{\exp(i\mathbf{k}\cdot\mathbf{r}_{12})}{r_{12}}$ with $\mathbf{r}_{12}$ defining the distance between the two points. Using the Kirchhoff boundary conditions [18] the amplitude at any point can be described with the Fresnel-Kirchhoff-diffraction integral

$$\mathbf{E}(\mathbf{P}_0) = \frac{A}{i\lambda} \iint\limits_\Sigma \left(\frac{\mathrm{e}^{i\mathbf{k}(\mathbf{r}_{12}+\mathbf{r}_{01})}}{r_{12}r_{01}} \cdot \left(\frac{\cos(\mathbf{n},\mathbf{r}_{01}) + \cos(\mathbf{n},\mathbf{r}_{12})}{2} \right) \right) dS. \tag{11}$$

where $\cos(\mathbf{n},\mathbf{r})$ defines the smaller angle between $\mathbf{n}$ and $\mathbf{r}$. The boundary Σ gives the limits of the aperture. This integral can be solved exactly.
Using the Fresnel approximation the $\cos(\mathbf{n},\mathbf{r})$ can be approximated as 1. Conditions for that are $x_1/z_i << 1$, $x_2/z_{01} << 1$, $y_1/z_i << 1$ and $y_2/z_{01} << 1$. Here (x_j,y_j) describes the point j on the plane of the aperture (j=1) and the image plane (j=2) with z_i the distance between both. Z_{01} is the distance from the aperture to the point source. So the point source is far away from the aperture in relative to its diameter ($z_i > \frac{1}{\lambda}\left(x_1^2 + y_1^2\right)$). Furthermore the distance r_{01} between the points P_0 and P_1 can be written[2] as

$$r_{01} \approx z_i \left(1 + \frac{1}{2}\left(\frac{x_0 - x_1}{z_i}\right)^2 + \frac{1}{2}\left(\frac{y_0 - y_1}{z_i}\right)^2 \right) \approx z_i. \tag{12}$$

With all those restrictions and approximations eq. 11 is

$$\mathbf{E}(x_0,y_0,,z_i) = \frac{\mathrm{e}^{ikz_i}\mathrm{e}^{i\frac{k}{2z_i}\left(x_0^2+y_0^2\right)}}{i\lambda z_i} \int\limits_{-\infty}^{\infty}\int\limits_{-\infty}^{\infty} \mathbf{E}(x_1,y_1)\,\mathrm{e}^{-i\frac{k}{2z_i}(x_0x_1+y_0y_1)}\,dx_1\,dy_1 \tag{13}$$

$$\hat{=}\mathbf{E}_0\frac{\mathrm{e}^{ikz_i}\mathrm{e}^{i\frac{k}{2z_i}\rho^2}}{i\lambda z_i} \int\limits_0^{\sigma} d\rho \int\limits_0^{2\pi} d\phi\,\rho\mathrm{e}^{-i\frac{k}{2z_i}\rho\mathrm{P}\cos(\phi-\Phi)}, \tag{14}$$

where polar coordinates ($x_0 = \mathrm{P}\cos(\Phi), y_0 = \mathrm{P}\sin(\Phi)$ and $x_1 = \rho\cos(\phi), y_1 = \rho\sin(\phi)$) are used for the second part. The aperture is assumed as circular with radius σ. Because of the symmetrical placement $\mathrm{P} = 0$ is a valid assumption as it will be the same for all angles.
Using the Bessel function of the first kind and first order with the general Bessel function of order m

$$J_m(u) = \frac{1}{2\pi i^{-m}} \int\limits_0^{2\pi} \mathrm{e}^{i(m\nu+u\cos(\nu))}\,d\nu \tag{15}$$

and the substitution $v = \frac{k\rho\mathrm{P}}{z_i}$ the integral for the amplitude (eq. 14) can be solved to

$$\mathbf{E}(x_0,y_0,,z_i) = \mathbf{E}_0\frac{\mathrm{e}^{ikz_i}\mathrm{e}^{i\frac{k}{2z_i}\rho^2}}{i\lambda z_i} ka^2 \left(\frac{2J_1\left(\frac{ka\mathrm{P}}{z_i}\right)}{\frac{ka\mathrm{P}}{z_i}} \right)^2. \tag{16}$$

[2] using a Cartesian coordinate system and a Taylor expansion

To get to the Airy disk three more definitions are needed. First the numerical aperture (NA)

$$NA = n\sin(\alpha) \approx n\frac{a}{f} = \frac{1}{2f/\#}, \tag{17}$$

where n is the refraction index, α the angle between the optical axis and the ray, f the focal length and $f/\# = f/(2a) = f/d$ the f-number (see [19] for more informations). Assuming the lens is in vacuum, for the refraction index it is used that $n = 1$. The second definition is the approach to dimensionless coordinates. The radial optical coordinate ν is defined as

$$\nu = \frac{2\pi a}{\lambda f} r_0 \approx \frac{2\pi}{\lambda} r_0 \sin(\alpha), \tag{18}$$

so the spot size r_0 will be smaller if the numerical aperture is larger for a given radial coordinate.
As last part the Fresnel number $N = \frac{\pi a^2}{\lambda z_i}$ gives a connection between the aperture area, the wavelength and the distance z_i from the aperture to the image plane.
Using that eq. 16 can be written as intensity distribution [20]

$$I(\nu) = (\pi N)^2 \left(\frac{2J_1(\nu)}{\nu}\right)^2 = I_0 \left(\frac{2J_1(\nu)}{\nu}\right)^2. \tag{19}$$

Figure 1 shows this Airy pattern for an aperture around the z-axis as a one-dimensional profile for a normalized intensity $I_0 = 1$. Most of the incident energy ($\sim 80\,\%$) is located in the central peak, so the higher-order peaks are faint with only small amplitudes. The proportionality in eq. 18 is a direct indication that a smaller spot size, so a smaller first minimum, means a higher resolution.

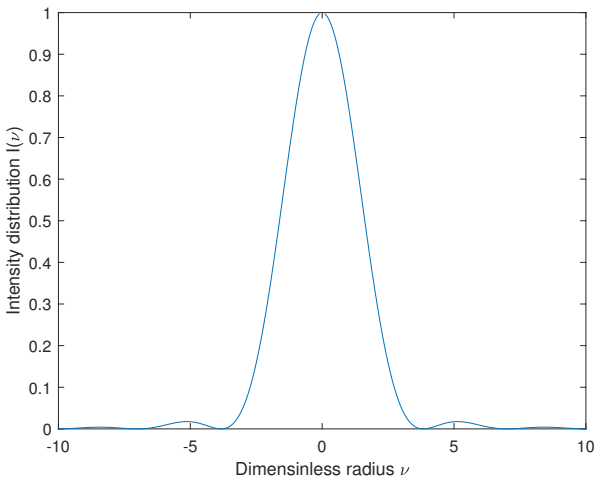

Figure 1: Normalized 1d- Airy disk for a circularly symmetric aperture. The intensity $I(\nu)$ is calculated with eq. 19 with $I_0 = 1$. The dimensionless coordinate ν is given by eq. 18.

2.3 Point spread function

The point spread function (PSF) is the response of the imaging system to a point source. In general an optical system can be defined with a two-dimensonal convolution [21]

$$g\left(x,y\right) = h\left(x,y\right) ** f\left(x,y\right), \tag{20}$$

where $f(x,y)$ is the input function, $g(x,y)$ the output function and $h(x,y)$ the transfer function. The two-dimensional convolution is represented with the symbol $**$. Using the convolution theorem this can be written as a Fourier transformation

$$G\left(u,v\right) = H\left(u,v\right) F\left(u,v\right), \tag{21}$$

with the frequencies u and v. $H\left(u,v\right)$ is called the optical transfer function (OTF), because its the only parameter dependent on the optical system, and is defined by

$$OTF \coloneqq H\left(u,v\right) = MTF \cdot \mathrm{e}^{i\Phi(u,v)}, \tag{22}$$

with the modulation transfer function $MFT = \left|H\left(u,v\right)\right|$. The OTF is also given by the PSF with

$$OTF\left(u,v\right) = \iint PSF \cdot \mathrm{e}^{ik(xu+yv)}\, dx\, dy. \tag{23}$$

If the input signal is a delta function $\delta\left(x,y\right)$ then output image can be described with the PSF

$$PSF \coloneqq g\left(u,v\right) = h\left(x,y\right) ** \delta\left(x,y\right) = h\left(x,y\right). \tag{24}$$

The transfer function is defined by eq. 19, so equivalent to the Airy disk. Similar to a Gaussian function, because the first-order peak can be approximated with such a function [22], a full width at half maximum can be defined. For a general Gaussian function $f\left(x\right) = a\exp\left(-\frac{(x-b)^2}{c^2}\right)$ the full width at half maximum is given by $FWHM = 2c\sqrt{\ln(2)}$. The function $f\left(x\right) = a\exp\left(-2\frac{(x-b)^2}{w^2}\right)$ (see also eq. 37) used in this thesis therefore has a value of

$$FWHM = w\sqrt{2\ln(2)} \tag{25}$$

for the full width at half maximum.

2.4 Rayleigh criterion

As stated before the numerical aperture can be used to determine the diffraction limit. A more precise approach can be made with the Rayleigh criterion. It gives a minimal distance two point sources can have to still be able to be resolved, as it is shown in Fig. 2. This is given when the first minimum of one PSF is at the same position as the maximum of the other [23]. Mathematical this is the case at the first minimum of the Bessel function ($J_1\left(\nu = 3.83\right) = 0$ [15]), so

$$r_{\mathrm{airy}} = 1.22\frac{f\lambda}{d} = 1.22\frac{\lambda}{2NA}. \tag{26}$$

A larger numerical aperture will result in a smaller minimal distance, hence a better resolution.

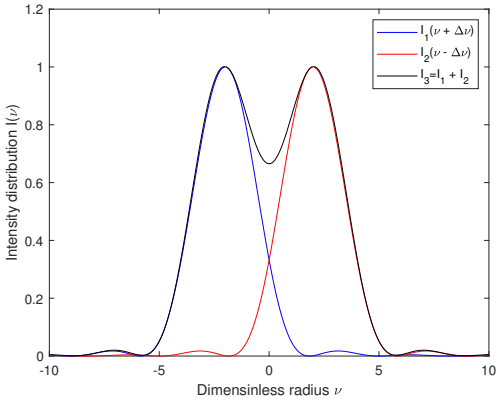

Figure 2: Intensity pattern for a system with two point sources which are resolved according to the Rayleigh criterion. The intensity distributions I_1 and I_2 are obtained with a normalized amplitude from eq. 19.

2.5 Aberrations

A real optical system will never produce a perfect, called aberration free, image. The whole system may not be perfectly aligned or lenses will have aberrations. This either means that the wavefront converging from the optical element is not spherical or that the focal length varies for different rays. Both will cause an increased spot size and a blurred image. In the following, chromatic and spherical aberrations, coma and astigmatism are discussed following the description made in [24].
The wavefront distribution in the exit pupil can be written as

$$W\,(x,y) = \frac{x^2+y^2}{2R} - \varepsilon_z \frac{x^2+y^2}{2R} - \varepsilon_x \frac{x}{R} - \varepsilon_y \frac{y}{R}, \tag{27}$$

where $\varepsilon = (\varepsilon_x,\varepsilon_y,\varepsilon_z)$ defines the center of curvature in the coordinate system (x,y,z) in the image plane. The origin has a distance R from the vertex of the exit pupil. The first term describes a spherical wavefront distribution with no aberrations, which means $\varepsilon = (0,0,0)$. The second term describes a defocussing of the wavefront to the image plane. Using the Rayleigh criterion a depth of focus

$$\varepsilon_z = \pm 2\lambda\,(f/\#)^2 \tag{28}$$

can be obtained for a diffraction-limited system. However this is only a rough estimation. The two last terms describe a transversal shift to the center of the wavefront in the (x,y)-plane.
Using a Taylor expansion in polar coordinates $x = \rho\cos(\theta)$ and $y = \rho\cos(\theta)$ with a normalized radial coordinate ρ to the edge of the exit pupil the wavefront distribution is

$$W\,(x_0,\rho,\theta) = \sum_{j,m.n} W_{k,l,m} x_0^k \rho l \cos^m(\theta) \tag{29}$$

with $k = 2j + m$ and $l = 2n + m$. Second-order wavefront aberration coefficients $W_{k,l,m}$ are also called Seidel aberrations.

Spherical aberration

Spherical aberration occurs when rays nearer to the optical axis have a larger focal length than rays further away. They correspond to a non-zero wavefront coefficient W_{040}. A circle of least confusion with a minimal spot size can be observed. It can be shown that the wavefront aberration at this point is $\Delta W = W_{040}(\rho^4 - 1.5\rho^2)$. The PSF will also not show

any higher order peaks, because these rays are focused more than the others, so appear in center of the first peak.

Coma

Coma occurs when the point source is not on the optical axis or when the lens has an angle to the incoming beam. This causes multiple 'foci' for a part of the beam when several, but not all, rays cross each other. Again a circle of least confusion can be found, but due to the multiple foci that is complex to describe mathematically. The 2d-PSF has a comet tail like shape which will be on the other side of the optical axis as the decentered point source. For a tilted lens the coma will appear on the side where the lens edge is closer to the circle of least confusion. The corresponding coefficient is W_{131} with an aberration term $\Delta W = W_{131} x_0 \rho^3 \cos(\theta)$ at the original focal spot.

Astigmatism

Astigmatism occurs when the point source is not on the optical axis. The same effect will also appear when a lens has different curvature for the x- and y- direction. This will cause a different focal length for the sagittal and the tangential (sometimes called meridial) rays. So two focal lengths where the spot size is minimal in one direction can be found. Both minima are also not located on the optical axis, but on the opposite site from the decenter of the point source. The circle of least confusion will be in between those two minima. Mathematically the astigmatism at this point is described by the wavefront aberration

$$\Delta W = W_{222} x_0^2 x^2 + \frac{\varepsilon_z h^2}{2R^2} \left(x^2 + y^2\right), \tag{30}$$

$$\varepsilon_x = -\left(\frac{2R}{h} W_{222} x_0^2 + \frac{\varepsilon_z h}{R}\right) x, \tag{31}$$

$$\varepsilon_y = -\left(\frac{\varepsilon_z h}{R}\right) y, \tag{32}$$

where W_{222} is the aberration coefficient and ε_i are the distances from the optical axis whith $i \,\epsilon\, \{x,y,z\}$.

Chromatic aberration

Chromatic aberrations occur when the beam is not monochromatic, so multiple wavelengths are present. Because the refraction index is wavelength dependent ($n\,(\lambda)$) every wavelength has its own focal length. A smaller wavelength (eg. blue light) has a smaller focal length than a higher (eg. red light) one. So if the image plane is located at the blue focus spot the image will have a blue dot and a yellow to red halo around it.

Strehl ratio

Another approach to describe an aberrated image is the Strehl ratio. It gives the ratio between the maximum intensity at the diffraction focus and the intensity maximum with no aberrations. The diffraction focus is at the point where the intensity is maximized for an image with aberrations, so where a minimal spot size occurs. This refers to the circle of least confusion as described in the sections above. The Strehl ratio S is given by the measured maximal intensity $I_{\text{diffraction focus}}$ and the maximal intensity of an unaberrated reference PSF $I_{\text{no aberration}}$ [24]

$$S = \frac{I_{\text{diffraction focus}}}{I_{\text{no aberration}}} = \frac{1}{\pi^2} \left| \int_0^{2\pi} \int_0^1 \mathrm{e}^{2i\pi\Delta W(\rho,\theta)} \rho \, d\rho \, d\theta \right|^2 . \tag{33}$$

So a Strehl ratio of 1 means that no aberrations are present in the observed image plane. The Maréchal criterion states that for a Strehl ratio $S > 0.8$ the image has no noticeable differences to an image with no aberrations [25]. Therefor this criterion can be used to determine if a system is diffraction limited.

3 Setup

In this chapter an overview of the setup is given and every part will be discussed in detail. The overall goal was to build up this test setup similar as possible to the actual experiment, where the objective will be placed. In Fig. 3 the schematic setup is shown. The light used has a wavelength $\lambda = 421\,\text{nm}$. The setup includes the coupling from a standard fiber to the scanning near-field optical microscopy (SNOM)-fiber with an tip aperture of 200 nm, which is chosen because of its point source like behavior. It is mounted on two one-dimensional translation stages and a piezo-controlled translation stage. Also the angle of the tip can be controlled in two dimensions. A second (damaged) fiber is used to control the initial alignment, as described in Sec. 3.8. The light is going through a window and the actual objective to test. The window is mounted on a translation stage together with the fiber. The objective is mounted on a two dimensional translation stage and with controllable angle adjustment. The collimated light out of the objective is redirected with a mirror through a lens mounted on a translation stage, to focus it down onto the camera. The view of the camera is shown in real time using the software supplied with the camera on the computer. Also the piezostage is controlled there.

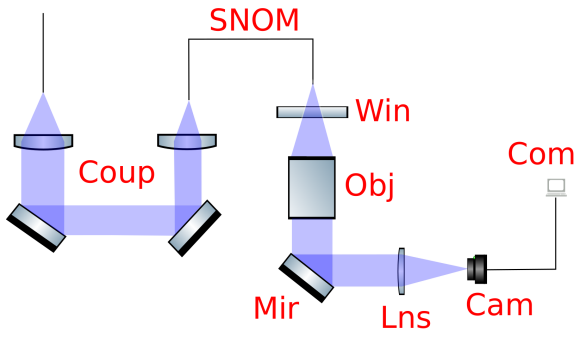

Figure 3: The experimental setup including: Coup: Coupling, SNOM: SNOM-fiber, Win: Window, Obj: Objective Mir: Mirror, Lns: Lens, Cam: Camera and Com: Computer

In the last part (Sec. 3.8) the procedure of the alignment is described. Later measurements and calculations have given an approximate power output of 10 to 40 nW. This low intensity is only detectable with the camera at a high-exposure time making a first, roughly correct placement and adjustment of the alignment with the SNOM-fiber nearly impossible. Therefore multiple steps are taken to improve the alignment and to always keep the beam pointed at the camera. An advantage of the whole setup is, that parts can be easily removed and realigned after all parts are inserted for the first time. Additional, swapping to another wavelength to test the 532 nm behavior can be done without touching the existing alignment. Only the coupling may need to be optimized again.

3.1 The fiber coupling

The laser light with a wavelength of $\lambda = 421\,\text{nm}$ is chosen because one of the main transitions from Dysprosium can be excited with that wavelength. Dysprosium has an open 4f-orbital with a ground state of ${}^5I_8$ determined by the Hund's rules [26]. This ground state has a strong transition $J = 8 \rightarrow J' = 9$ under the absorption of light with a wavelength of $\lambda = 421\,\text{nm}$. A strong transition means a broad linewidth in the spectrum and allows precise imaging of the atoms. It was planned to swap that laser with another one with wavelength $\lambda = 532\,\text{nm}$, the other relevant wavelength in the later experiment affected by the objective, and also test it under this condition. This wavelength is used to model and adjust the potential-landscape around.
In Fig. 4 the coupling is shown. From the light generation to my setup a polarization-

maintaining single mode fiber[3] is used. The output of the fiber is collimated and with two mirrors directed to the SNOM-fiber, where it is focused into the core of the fiber with another lens.

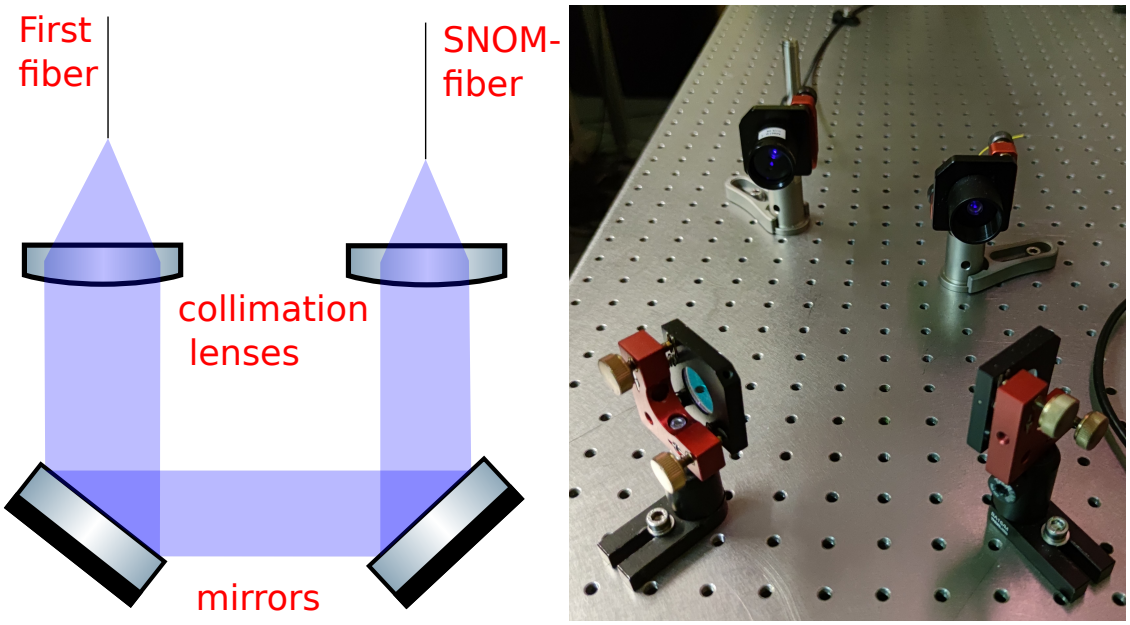

(a) Schematic setup

(b) Experimental Setup

Figure 4: a) Schematic and b experimental setup of the coupling into the SNOM-fiber. The collimated beam gets focused into the core of the fiber with two mirrors.

First a dummy fiber was used to get the base coupling, which was then swapped out for the SNOM-fiber. Then the coupling only needed to be readjusted by a small amount.

3.2 The SNOM-fiber

The atoms in the actual experiment will emit light in all directions. To imitate that a point-like source is needed. Felix Kleißler [11] shows that a SNOM-fiber with an aluminum coated tapered tip is working well for measuring the PSF. The results obtained with a small fiber aperture are significant better than those from a very small pinhole. Also these fibers are commercial available in contrast to the pinholes he developed by himself. Therefore, a SNOM tip that is made by pulling a SM400 fiber[4] is chosen. The fiber tip has an aperture of 200 nm and is very fragile. To not damage it the fiber is inserted into a fiber clamp[5] in a way that the coating is in free space and passively fixed in its position and angle.
With a kinematic mount[6] the angle control can be done with 0.75° per revolution. The fiber holder then is mounted together with the window on a translation stage with 500 µm per revolution[7]. An individual mounting on another translation stage with a resolution of 10 µm[8] provides freedom in the distance between the window and the tip. To be able to control this distance more precisely a Piezoelectric translation stage[9], controlled by a KPZ101 Cube, with a theoretical resolution of 0.76 nm is placed on to of this translation stage. All of this mounting is shown in Fig. 5. This all together allows fine adjustments of the beam path (from now on called the z-Direction).

[3] Thorlabs: PM S405XP
[4] Fiber used: E50-SM400-AL-200
[5] Thorlabs: SM1F1-250
[6] Thorlabs: KM05T/M-SM05
[7] Thorlabs: XR25P/M
[8] optics4u: TS25
[9] Thorlabs: NF15AP25/M

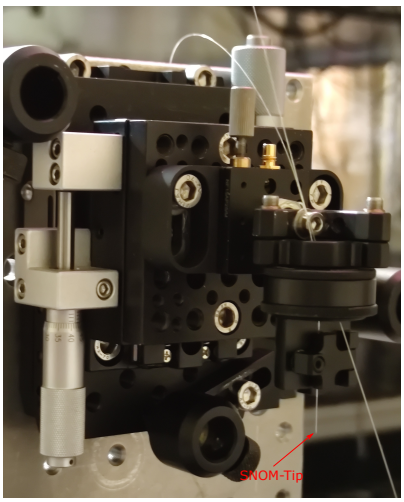

Figure 5: The mounted SNOM-fiber with another (damaged) fiber for the alignment. The tip is mounted such that the coated tip is in free space to prevent damage and the z position can be changed precisely with the piezo-stage. The additional translation stage allows for a coarse placement and to scan a larger areas faster. The window can be mounted below in the post holder.

Such a precise control over the position is needed for further measurements as discussed in Sec. 4.1. Originally it was planned to mount the objective onto the piezostage, but because of its weight restriction and not enough space to mount it safe the fiber instead was picked to be adjusted for the z-direction distances.
The SNOM-fibers have a damage threshold of 400 µW before the Aluminum coating is damaged. With an expected transmission efficiency of $10^{-4} - 10^{-6}$ this results in a low power output making the alignment complicated because the beam can only be detected with the camera. Therefor another SNOM-fiber, that was damaged in an early try, is used to achieve a first, preliminary alignment.

3.3 The window

A window[10] is included as viewport in the test setup identical to the actual experiment. The objective is designed to account for the additional refraction caused by it. The window is mounted together with the fiber onto the z-direction translation stage.

3.4 The objective

The objective is a custom design to match the exact conditions in the experiment. That means for a correct placement the light will be collimated after passing through it. In the corresponding Zemax file the distances between window and objective are given as 7.503 mm for 421 nm and 8.05337 mm for 532 nm. To place the objective in the right position and control the angle as well as be able to deliberately misalign for testing of the diffraction limit it is placed on a translation stage with a vernier reading of 1 µm[11] and a mirror mount[12] with a resolution of 150 µm/turn $\hat{=}$ 0.107°/turn. With eq. 17 the objective has an $NA = \frac{30\,\text{mm}}{2 \cdot 30\,\text{mm}} = 0.5$. That means the smallest distances between two points to be resolved, according to the Rayleigh criterion (eq. 26), are $d = 514\,\text{nm}$ and $d = 649\,\text{nm}$ for $\lambda = 421\,\text{nm}$ and 532 nm respectively.

[10] Thorlabs: WG41050-A
[11] Newport: M406 with SM-13
[12] Radiant dyes: MXI-2-3030z

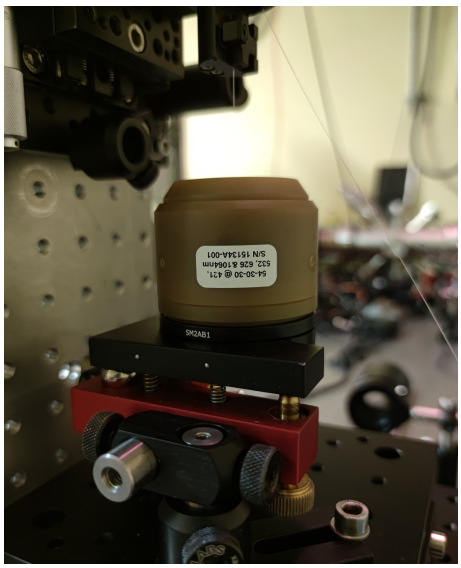

Figure 6: The objective placed in the test setup below the SNOM-fiber.

3.5 The mirror

A mirror[13] is added to redirect the light through the second lens. It is mounted in the same mirror mount as the objective, so the path of the light can be controlled in a way that the alignment of the lens and the camera can be done more easily.

3.6 The second lens

The required resolution $\Delta f = 513.62\,\text{nm}$ is calculated with the Rayleigh criterion from eq. 26 at wavelength $\lambda = 421\,\text{nm}$ and an $NA = 0.5$. To measure the PSF of a beam at least 2 pixels on the camera need to be covered by it. To make a more valid statement of its shape 3 pixels are assumed in the following. These values are a result out of the Nyquist criterion [27] giving a limit what frequencies, in frequency space, can be reconstructed from a set of data. With a pixel size of 13 µm from the camera the required magnification is $M = \frac{\text{pixel size} \cdot 3\,\text{pixel}}{\Delta f} = \frac{13\,\mu\text{m} \cdot 3}{513.62 \cdot 10^{-3}\,\mu\text{m}} = 75.93$.
All lenses tested as described in the following are achromats to reduce spherical and chromatic aberrations (Sec. 2.5) and are coated for $\lambda = 421\,\text{nm}$. Doing a thin lens approximation to determine the needed focal length is valid for a rough estimation, but will not calculate the exact value due to the non-zero thickness of both the objective and the achromat lens. With the thin lens equation

$$\frac{1}{f} = \frac{1}{\mathrm{d_O}} + \frac{1}{\mathrm{d_I}} \tag{34}$$

where $\mathrm{d_O}$ and $\mathrm{d_I}$ are the distances to the object and the image plane respectively and a Magnification

$$M = \frac{\mathrm{d_I}}{\mathrm{d_O}} = \frac{f_2}{f_1} \tag{35}$$

the required focal length is $f = 2250\,\text{mm}$. In eq. 35 the second equality is only given when the beam from the first lens is focused at infinity, because then the distance between the lenses doesn't matter. The obtained focal length matches the value of the simulation done with the Zemax optimization tool (see [28] chapter 8 for more information) of $f = 2243.1\,\text{mm}$. Lenses with such a large focal length need to be custom made, the same applies for a mount. Using another option to focus the beam onto the camera will make the building part of the setup easier.

[13] Thorlabs: BB2-EO2

A second possibility is to use a system with two lenses, which result in lower focal length for both lenses and are therefore more readily availible. To not lose any rays it should be $f_1 > f_2$, so a higher intensity is maintained and an easier detection is possible. As shown in Fig. 7 a larger focal length for the first lens will reduce the spot size. The expected spot size for a magnification of $M \approx 75$ is $\Delta f \cdot M = 38.5\,\mu\text{m}$. The Rms radius for the zero field and a focal length of $f_1 = 1000\,\text{mm}$ is approximately double the size than the expected spot size. The field component here refers to a point in (x,y) space with the origin at the optical axis. However the exact values from the simulations are not usable, because they are not fully optimized. Further simulations show that a spot size around 45 µm can be achieved. The focal length of the second lens does not have a large effect on the spot size especially if the size is already optimized with the first lens. So the second lens can be chosen freely.

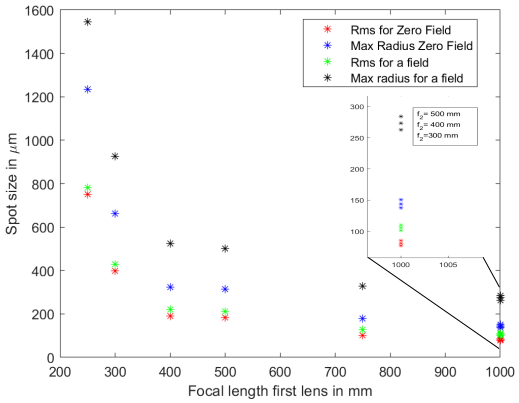

Figure 7: Spot size comparison for different focal lengths for both lenses according to the simulation. Rms refers to root-mean-square radial size. A non-zero field means that the object is moved by 0.1 mm in y-direction.

Another parameter important for the alignment and first placement of the components of the system is the sensitivity. It is a value that describes the distance the focal length needs to be shifted if the distance between the two lenses is varied. The sensitivity is given by

$$\begin{aligned}\text{Sensitivity} &= \frac{f(x+\Delta x) - f(x-\Delta x)}{2\cdot\Delta x} = \frac{(d+\Delta d_{\text{smaller}}) - (d-\Delta d_{\text{bigger}})}{2\Delta x} \\ &= \frac{\Delta d_{\text{smaller}} + \Delta d_{\text{bigger}}}{2\Delta x},\end{aligned} \tag{36}$$

where d is the distance between second lens and the image plane and Δd the adjustment made for a movement of the first lens by the distance Δx. A lower sensitivity means that finding the focus is easier, because the placement of the lenses and the camera can be less precise. Fig. 8 shows that again a larger focal length for the first lens reduces the sensitivity and the focal length of the second lens has only a minor impact on the result.

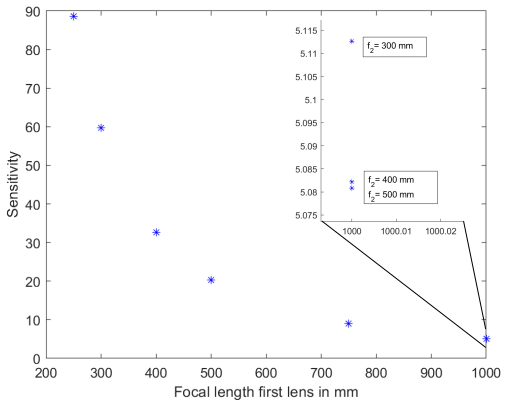

Figure 8: Sensitivity comparison for different focal length for both lenses in this system. Calculated with eq. 36 from the distances gained out of simulations

The problem with a two lens setup is the diffraction limit. With all tested lenses the setup was already near the diffraction limit in a perfect, meaning not misaligned, state. That reduces the ranges that are provided with a single lens, so reduce the overall performance of the objective. Another, but minor, problem is the large overall distance of more than 3 m. This is not practical to work with in the actual experiment[14] and so another solution was chosen.
Because in the test setup a different camera (see Sec. 3.7) with a smaller pixel size of 1.85 µm only a magnification of $M = 10.8$ is needed to cover 3 pixels. The chosen lens[15] has a focal length of $f = 750\,\text{mm}$ which results in a magnification of $M \approx 25$ (according to Zemax simulation: $M = 25.0798$). With this setup the actual experimental one is not exactly copied, but it is sufficient to investigate the behavior of the objective and determine its diffraction limit.
The lens is mounted on a translation stage[16] with a resolution of 10 µm to adjust the focus onto the camera.

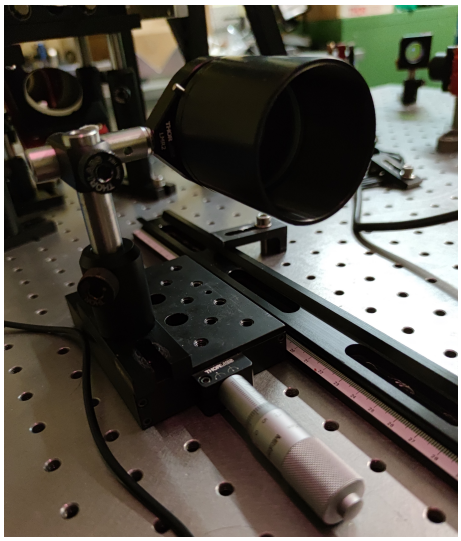

Figure 9: The used lens mounted on a tranlation stage together with an iris for easier alignment

An iris directly in front of the lens is used to align the lens to the camera. For that the

[14] A negative focal for the length first lens could solve that problem, but a custom made one would be required
[15] Thorlabs: ACT508-750-A
[16] Thorlabs: PT1/M with 150-801ME Actuator

lens can be moved freely in the (x,y) plane as well as be rotated (Fig. 9). The ruler seen in the background is used to move the lens over a larger distance while still keeping the alignment of the beam. Using that, the region around the focus can be scanned quickly to determine a good starting position for more precise measurements.

3.7 Beam profile imaging

To image the beam a FLIR Blackfly S[17] with a pixel size of 1.85 µm x 1.85 µm is used. With the associated software (Spinnaker V2.0.0.146) a real time image can be observed and the settings such as the exposure time can be adjusted. The camera also supports different gamma values, but to avoid distortion of the image it is always set to 1 (see [29] for detailed info on the gamma value). Also the alignment can be adjusted in real time.

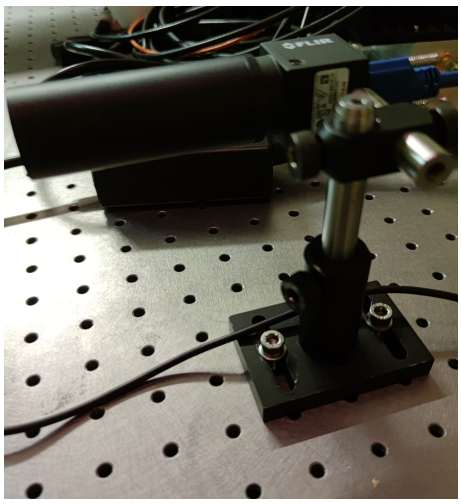

Figure 10: The mounted camera in the setup, the lens tube blocks background light from the sides.

The camera is mounted the same way as the lens, so it can be rotated and translated in x- and y-direction (Fig 10). Note that images on the computer screen are rotated by 90°, because of the way the camera is mounted. Also an iris in front of it is used again for the alignment. A translation stage is not needed because the focus is controlled with the position of the lens.

3.8 Alignment and progress of the system

First only the fiber, that is later used to couple light into the SNOM-fiber, and the camera are aligned to each other. This is done by two iris in front of the fiber and the camera. The position of the camera is adjusted so that the beam is centered trough the iris and the back reflection, coming from the ND filter to protect the camera from to height power density, is parallel to the incoming beam by adjusting the tilt of the camera. This steps are iteratively done until both parameters are optimized. Then the objective is inserted and moved in the (x,y)-plane and rotated around the axis until both parameters are optimized again. The beam out of the objective is then collimated by adjusting the distance to the light source and using a shear interferometer[18]. Both of this must be done with the camera near the light source to detect it. To place the second lens in the system the camera then is moved and realigned at its final position. Then the same steps as for the objective are done to place the second lens at the right angle, now with an iris in front of the lens. The distance to the camera is then adjusted to focus the beam onto it. As last part the window is inserted and adjusted as well. Because there where problems with the

[17] FLIR: BFS-U3-120S4M-CS
[18] Thorlabs: SI254

right angle of it, the decision to do further progress without the window was made. The angle couldn't be controlled well enough to remove all non symmetric behavior. With only the fiber, in its lens tube, there is not enough space to place a mirror mount with angle control in the setup. This problem is solved when the SNOM-fiber is used instead of the dummy fiber, because of its different mounting architecture. However it turned out that the window is not affecting the position of the beam on the camera, even with a large tilt, so it is no issue to postpone the placement of the window.
After this first alignment a pinhole[19] with a diameter of 1 µm is inserted and placed at the right position and angle, so that the beam is centered on every optical element. With the pinhole positioned all other elements are now checked and adjusted by a small amount, if necessary, to minimize the spot size and aberrations. After this the system is defined as optimal, what my be not the actual case but is taken as reference state.
Then the pinhole, together with the dummy fiber illuminating it, is removed and the SNOM-fiber inserted. Swapping to the SNOM-fiber requires coupling into it and a re-alignment of the fiber holder, because some parts needs to be removed to place the fiber in it. To not loose the signal an additional SNOM-fiber, that was damaged in a first try and therefore had a higher output, is used to do another alignment. Both fibers are inserted through the mount with the non tip side to decrease the possibility to hit and damage the tip. Then the first coupling is done with a dummy fiber and adjusted for the damaged fiber after that. With enough light going trough the fiber to detect it the realignment of the holder is done. And as last step the damaged fiber is replaced with the non-damaged one, with as little as possible displacements to the holder. Then the coupling is optimized and the distance between tip and objective adjusted, so that a collimation is achieved. Because the beam can't be detected with the Shear interferometer, the spot size on the camera is minimized. This is a correct relation due to this whole procedure. As last part of this the tilt of the fiber is optimized to remove all aberrations. Then the window can be inserted and aligned again.

[19] Thorlabs: P1H

4 Simulation of the diffraction-limited system

To understand the expected behavior of the setup simulations were performed in Zemax[20]. In particular, it was investigated how an image is affected by deliberate misalignments of the optical components and how accurate these components need to be placed for a diffraction limited image. As coordinate system assumed for the simulations, the optical axis is defined as z-axis and is orthogonal to the (x,y)-plane. The direction of x and y does not matter, because of the rotational symmetry, so they are chosen arbitrary. In principle all parts of the setup can be displaced in all directions and rotated around all axis, but in the following only the misalignments that can be realized in the test case and are relevant for the experiment are covered. Also most displacements can be compensated by a deliberate misalignment of another parts leading into a optimal positioning for that set of parameters. Because the large amount of parameters that can be adjusted this is only discussed briefly at the end for a compensation between the focal distance of the objective and the focal distance of the second lens.
The general settings used for all simulations are a wavelength of $\lambda = 421\,\mathrm{nm}$, an aperture value of $0.5\,\mu\mathrm{m}$, three fields[21] with (0,0), (0,0.07) and (0,0.1) and Real Ray aiming. The different fields are included here, because in the actual experiment multiple atoms are imaged at the same time. Not all of them will be on the optical axis.
The PSF, mathematically described by eq. 19, is the most useful transfer-function to characterize this system. One advantage is that it can be directly compared to images taken in the test setup, by comparing both the Strehl ratio (Sec. 2.5) and the full-width at half maximum (FWHM, see Sec. 2.3). Both values are determined by fitting a Gaussian function

$$f(x) = S \cdot \exp\left\{-2 \cdot \frac{(x - x_0)^2}{w^2}\right\} + C \tag{37}$$

to the data points, where w the waist and S is the amplitude, which is equivalent to the Strehl ratio for the simulations, because of the way Zemax calculates the amplitudes this is already normalize to the unaberrated function. This is a good approximation according to the test sample shown in Fig. 11 and more theoretically proven in [22]. With $\mathrm{FWHM} = w \cdot \sqrt{2 \cdot \log(2)}$ the full width half max is calculated and compared. A third option to analyze would be the Airy disk radius, defined by the position of the first minimum, but this is often less practical to measure. A diffraction-limited system is given for the Maréchal criterion (see [25]) with Strehl ratio > 0.8 or by the Rayleigh criterion (eq. 26) $d < 1.22 \cdot 421\,\mathrm{nm} \cdot 25 = 12.84\,\mu\mathrm{m}$. A diffraction-limited system due to the Rayleigh criterion can be stated from the RMS spot radius at the focus from the simulations. Also in the test setup the quality of the initial alignment will affect the determined diffraction limited range of the system for one measurement cycle. The process must be done iteratively to find the total best position. This is not necessary for the simulations.

[20] see [28] for all features and detailed explanation how to use it
[21] field correspond to coordinates (x,y) in mm for the object placement, where z is the optical axis

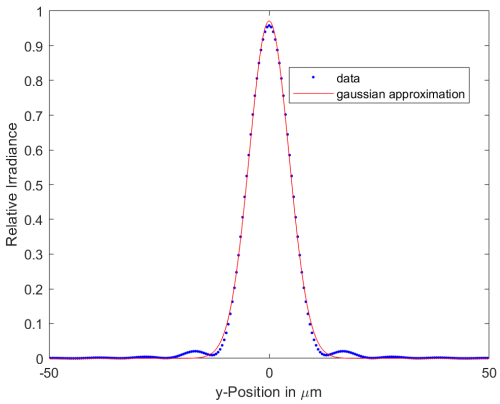

Figure 11: Gaussian model to describe the PSF of an Airy disk with fit parameters: $S = (0.97 \pm 0.002)$, $x_0 = (0.010 \pm 0.001)$ µm, $w = (8.98 \pm 0.02)$ µm and $C = (0.00 \pm 0.007)$. The data fitted here is a test sample from the simulations.

4.1 Movement of the point source

A change of the distance between the point source and the window will have an effect on the collimation out of the objective. Moving closer to the the window will result in a diverging beam and moving further away from the window will focus down the beam. As seen in Fig. 12 the PSF is a function of the distance.

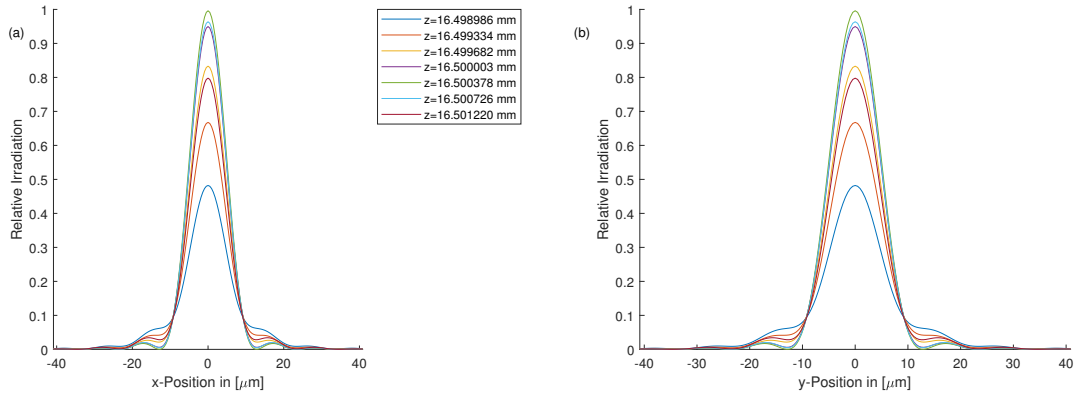

Figure 12: Simulated 1d-PSF in (a) x- and (b) y-direction for a change in the distance between SNOM-fiber and window. For a better visibility only a part of the simulated data is displayed.

The PSF in x- and y-direction has the same shape for a specific positioning of the point source, because the Airy-disc and the setup are rotationally symmetric. Also the general Gaussian shape will not change, because variations along the fixpoint axis will not result in a change of symmetry.
Using eq. 37 as fit function the Strehl ratio and the FWHM are extracted and plotted against the distance (Fig. 13). Again the symmetry in x- and y- direction with a maximum or minimum for the Strehl ratio or the FWHM respectively can be seen.

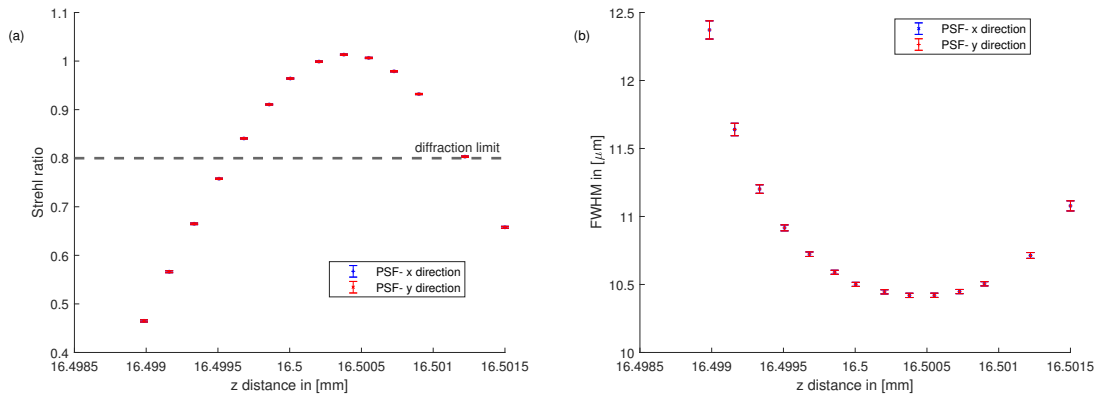

Figure 13: (a) Strehl ratio and (b) FWHM, calculated with eq. 37, dependent on the point source distance to the window. Errorbars are calculated out of the fit error.

From the criterion $S > 0.8$ for a diffraction-limited system a range of 1.62 µm can be determined with a best position for the point source at $z = 16.50038$ mm. With a size of the point source of 0.5 µm the magnified spot diameter is ~ 25 µm. The minimum of the FWHM is, as expected, approximate half the spot diameter with 10.42 µm, although that is only an indicator for a correct simulation and not an exact value for a statement of the quality. Also the best position of the light source is confirmed.
The spot radius in dependent of the distance between the point source and the window is shown in Fig. 14. The range for a diffraction-limited system here is ~ 2.5 µm, differing to the smaller range of 1.62 µm due to the different criteria used.
The optimal position for the smallest spot radius is 16.5002 mm, which is similar to the result from the Strehl ratio.

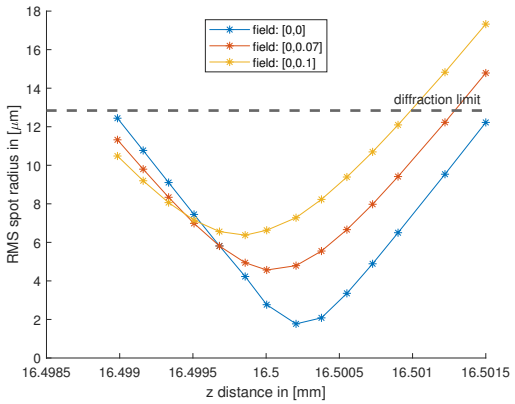

Figure 14: RMS spot radius at the focus for different field components and a movement of the point source along the z-direction.

For a decenter of the point source by $\Delta y = 0.1$ mm a minimal spot size is achieved by moving the source ~ 350 nm closer. The aberration caused by the off axis placement is compensated by effects from the not fully collimated beam. Important to notice is that a change of the diffraction limit due to the changed f/# number for an off axis point source is ignored in the simulations. To achieve these results in the test setup a very precise control is needed and therefore a piezo stage is included in the setup.
A point source is isotropic, so there is no need in analyzing a tilt of it. However a SNOM-fiber has a preferred direction which will result in limitations of the test setup showing this characteristic and need to be taken in account.

4.2 Tilt of the window

Because the window is just a flat glass-plate, decentering it in the (x,y)- plane will not change the beam at all. Only a large decenter where not all light passes trough the window will have an effect.
Also here is only the positive rotation along the y- direction for a zero field point source is discussed. As the Airy disk and the system are rotationally symmetric the effect of a rotation along the x- direction is identical to a rotation around the y- direction. For a field not on axis this is not the case anymore, but this is too much for the scope of this simulation part, so only a field along the tilted axis is looked at for the spot radius.
As expected the PSF is no longer the same in the x- and y-direction. The PSF in the y-direction is still symmetric around the origin, because the rotation is also along this axis (Fig. 15b). For the PSF along the x-axis the maximum changes the position (Fig. 15a) with $+56\,\mu m/1°$. Also the second order peak on the positive side of the x-direction has a higher relative irradiation compared to the peak on the negative side indicating coma. So the PSF in x-direction is no longer symmetric.

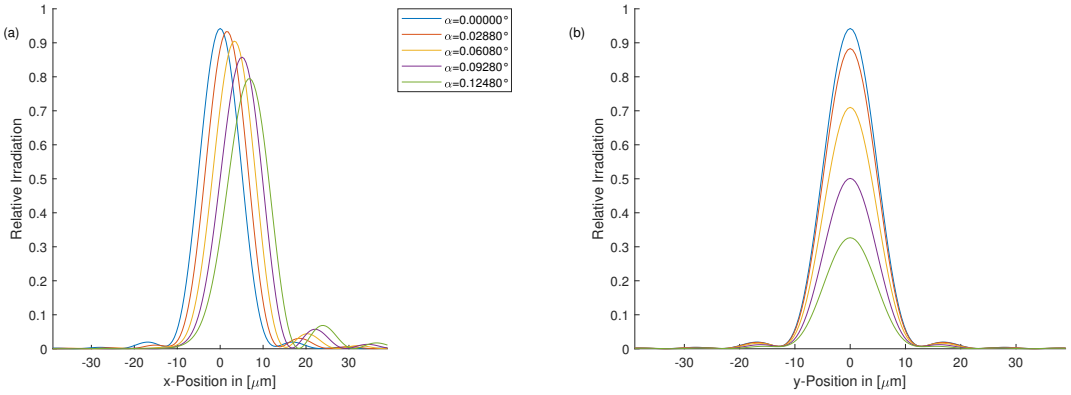

Figure 15: Simulated 1d-PSF in (a) x- and (b) y-direction for a tilt of the window around the y- axis.

Also the Strehl ratio decrease is not symmetric for x- and y-direction. While the system is diffraction limited for 0.125° in the x-direction the limit is reached at 0.048° for the y-direction (Fig. 16a). The limits are not similar due to the fact that one direction is parallel (y-direction) to the tilt-axis and one is orthogonal (x-direction). That means for rays with a fixed y-value and a variable x-value they have different refraction angles. According to D. Stack [30] this will vary the focal length if the tilted object is a lens. In theory, the here used flat window has a focal length of infinity, but a real one will always have a curvature and therefore a finite focal length. This means an angle between the window surface and the optical axis can effect this distance. If the x-value is fixed and the y-value is variable the angle will only change by a small amount and therefore the focal distance has also only a small variation.
In Fig. 16b the FWHM is shown. For the x-direction it increases continuously. For the y-direction is has a minimum at 0.095°. But this minimum is located out of the range where the system is fully diffraction limited, so it is not relevant for this analysis. Also the increase of the x-direction FWHM exceeds this decrease and will result in an overall increase. The occurrence of this minimum is not fully clarified, but could be an effect of chromatic aberrations. The window is not designed for a specific wavelength, but to minimize all aberrations for a larger wavelength range.

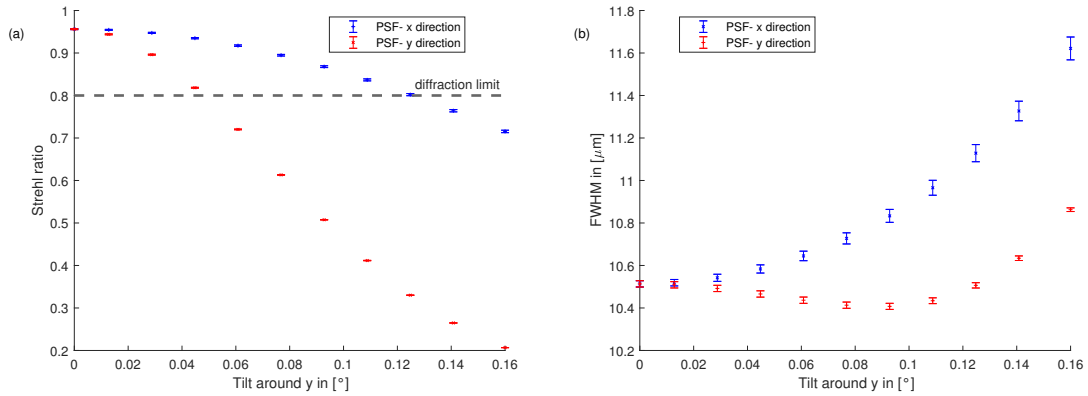

Figure 16: (a) Strehl ratio and (b) FWHM, calculated with eq. 37, dependent on the tilt of the window around the y-axis. Errorbars are calculated out of the fit error.

In Fig. 17 the RMS spot radius will increase for a larger angle between the optical axis and the plane of the window. This validates that the minimum will not cause a general decrease of the spot radius for a tilted window. So the minimum of the spot radius is at 0.000° with a range of 0.131°(field) − 0.147°(no field) to be diffraction limited. This value is again different to the range for the Strehl ratio, because both methods are again different criteria. For a orthogonal window the difference of the spot radii between an on axis point source and a decentered field is $\sim 3.5\,\mu m$. The compensation between the tilt of the window and the decentered field causes this difference to decrease to $\sim 1\,\mu m$ at the diffraction limit. If the window is tilted by an even larger amount this will cause a smaller spot radius for a misplaced point source. For further considerations this is not important here, because the system will not be diffraction limited at this constellation.

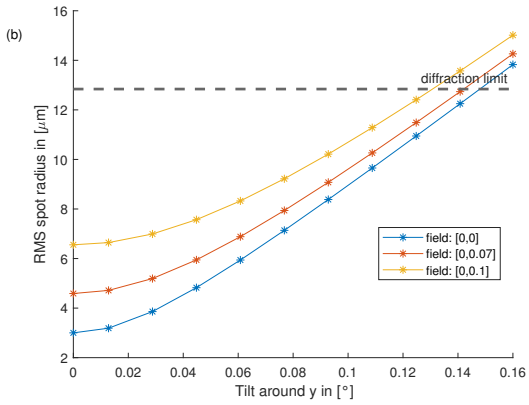

Figure 17: RMS spot radius for different fields in dependent of a tilt around the y-axis.

So, as expected, placing the window orthogonal to the z-axis gives the best result.

4.3 Distance between window and objective

A change in the distance between window and objective, as discussed in the following, will not affect the distance between window and point source ot the distance between the objective and the second lens. A relative movement of the window between point source and objective has little to no effect and is therefore not discussed here and also because in the actual experiment this cannot be adjusted easily.
As the movement is done only along the z-direction, the PSF for x- and y- direction is identical as it can be seen in Fig. 18. Also the PSF is symmetric around the z-axis due to

the same reason. With Fig. 19a a range of 1.64 µm for a diffraction-limited system from the Maréchal criterion is determined.

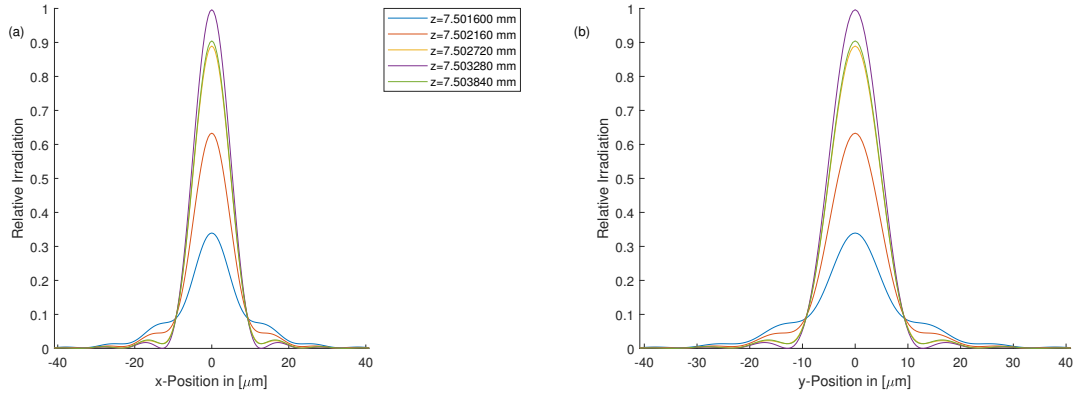

Figure 18: Simulated 1d-PSF in (a) x- and (b) y-direction for a change in the distance between window and objective.

The optimal position is at 7.5033 mm, which is close to the value of 7.503 mm given by the manufacturer. The FWHM (Fig. 19b) gives a minimal radius for 7.5034 mm. The value of the minimum is 10.42 µm. The minimum of the FWHM verifies the optimal distance for the objective from the window (Fig. 20).

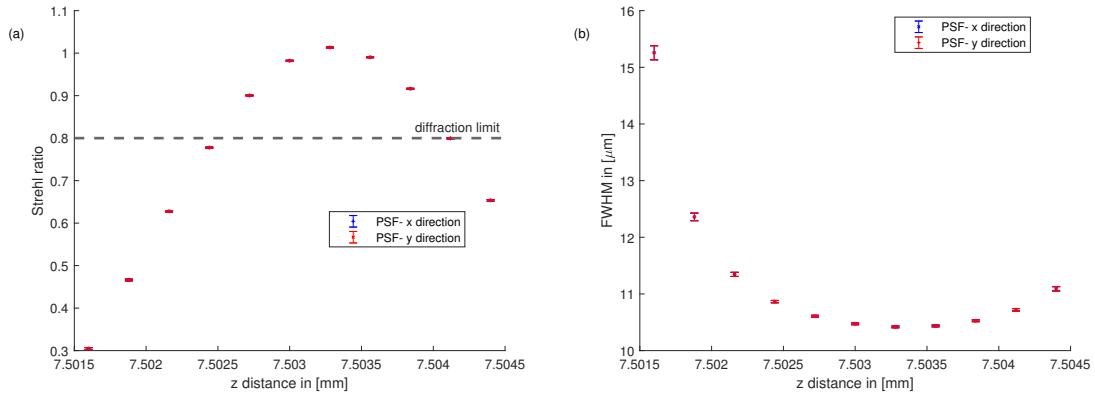

Figure 19: (a) Strehl ratio and (b) FWHM, calculated with eq. 37, dependent on the objective distance to the window. Errorbars are calculated out of the fit error.

According to the Rayleigh criterion the range to place the objective is 2.47 µm for a diffraction-limited system. For a field of 0.1 mm along the y-direction to have a minimum of the spot size the objective needs to be moved 380 nm closer to the window.
All these values are similar to those from the evaluation of the movement of the point source in Sec 4.1, that means it doesn't matter which distance is changed the effect will be the same.

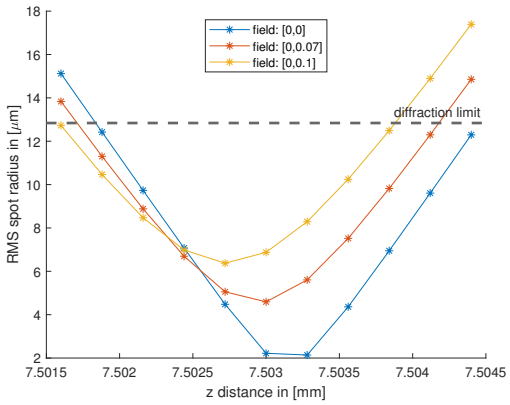

Figure 20: RMS spot radius for different fields in dependent of the distance between window and objective

4.4 Decentering of the objective

The symmetry of the system will cause the same absolute value for a decenter in positive y-direction on the y-axis as a negative decenter will have in the opposite direction. And the same values will occur for the x-axis if the decenter is done in x direction. So it is sufficient to analyze only one particular misplacement to know the behavior for a decenter in all directions. A displacement in positive y-direction will cause the PSF in y-direction to move by $-64\,\mu m/1mm$, so against the displacement direction. Also a slight increase of the second order peak is observable (Fig. 21), so a presence of coma. The x-direction PSF is symmetric around z-axis for movements and only decreasing in the relative irradiance for higher displacements, because it is orthogonal to the decenter.

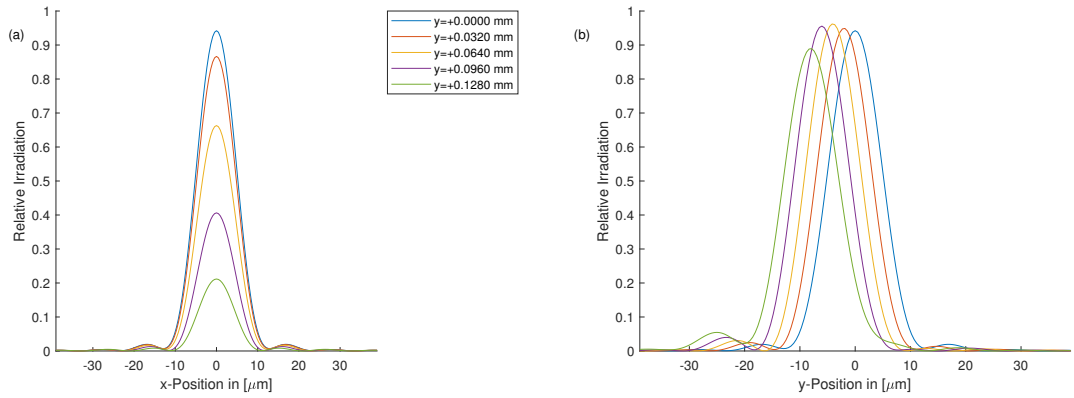

Figure 21: Simulated 1d-PSF in (a) x- and (b) y-direction for a decenter of the objective in y- direction.

The Strehl ratio in Fig 22a shows that the system is diffraction limited for a range of 0.046 mm(x-direction) and 0.147 mm(y-direction). So the movement has a larger effect on the irradiance of the orthogonal PSF and can be explained by the movement along a non symmetry axis of the system resulting in a non symmetric behavior. The Rayleigh criterion gives a diffraction-limited system for a displacement up to 0.158 mm with an optimal position centered on the z-axis, as expected. The minimum of the spot size will move with the misplacement of the point source, because the point source is then again placed directly on the new optical axis after the adjustment.

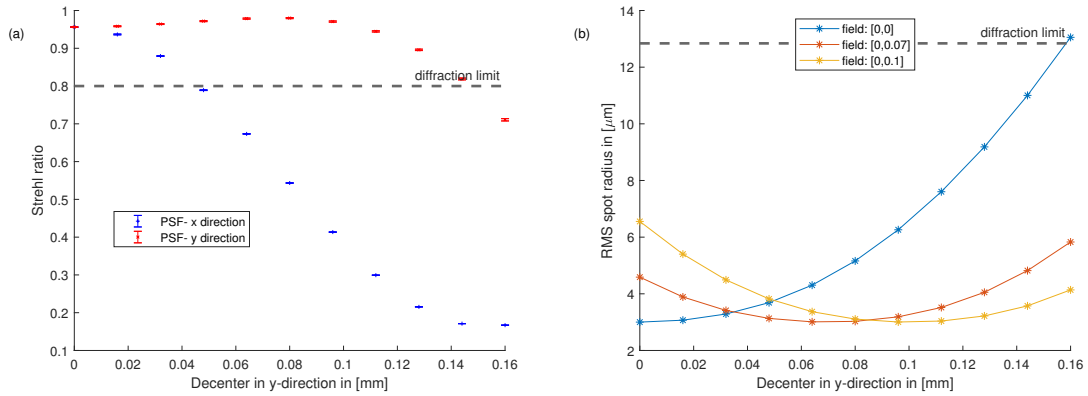

Figure 22: (a) Strehl ratio, calculated with eq. 37, and (b) RMS spot radius dependent on the objective decenter in y-direction. Errorbars are calculated out of the fit error.

4.5 Tilt of the objective

Similar to Sec. 4.2 it is sufficient to simulate only one rotation. However, in the test setup the tilt around both axis should be analyzed to determine if the objective is properly manufactured. For the window that is not necessary, because it is not the one that will be used in the experiment.
Also similar to a tilt of the window is the PSF for both directions (Fig. 23). The y-direction one is always symmetric around the z-axis and only a decrease in the Strehl ratio is observable. The x-direction is shifted by $+54.3\,\mu m/0.1°$ and not symmetric around the maximum.

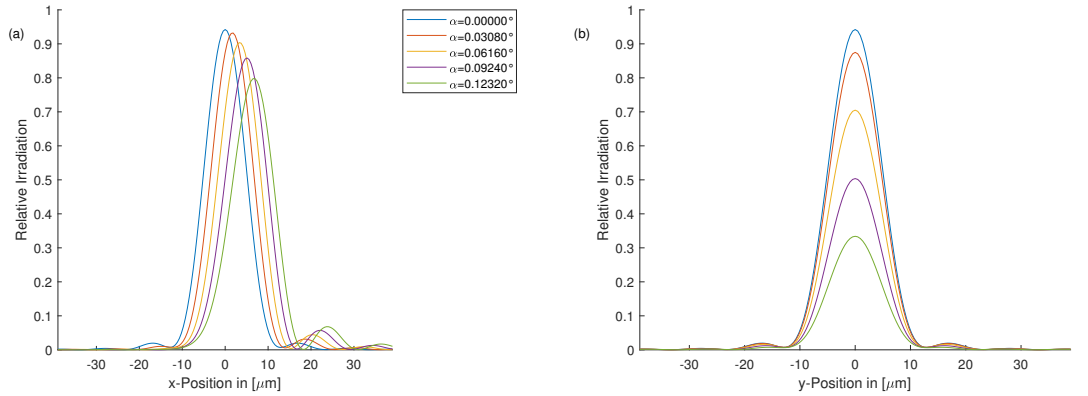

Figure 23: Simulated 1d-PSF in (a) x- and (b) y-direction for a tilt of the objective around the y- direction.

As seen in Fig. 24 a tilt around an axis along one measured direction will again cause a difference for the parallel direction and the orthogonal one. The ranges for a diffraction-limited system are 0.126° and 0.048° for the x- and y-direction respectively. The small minimum in the y-direction FWHM is compensated by the increase in x-direction and is also out of the limits of a diffraction-limited system.

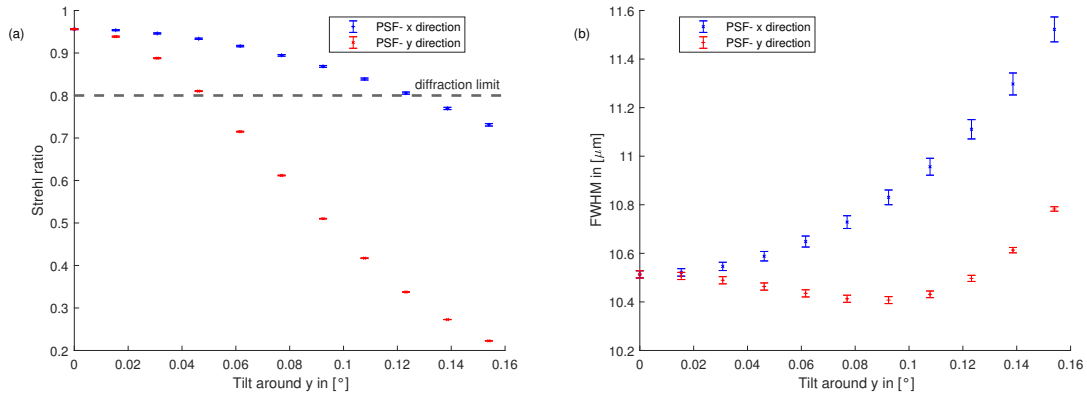

Figure 24: (a) Strehl ratio and (b) FWHM, calculated with eq. 37, dependent on the objective tilt. Errorbars are calculated out of the fit error.

The spot radius is minimized for an orthogonal placed objective with a range of 0.145° to be diffraction limited (Fig. 25) and a misplaced point source will compensate the effect caused from the tilt. That means there is a point, beyond the diffraction limit, where a deliberately non-centered point source has a smaller spot size, but that constellation will not represent the global optimal position and will cause aberrations such as coma. Most dominant to be observed in the PSF for the x-direction with only a small tilt.

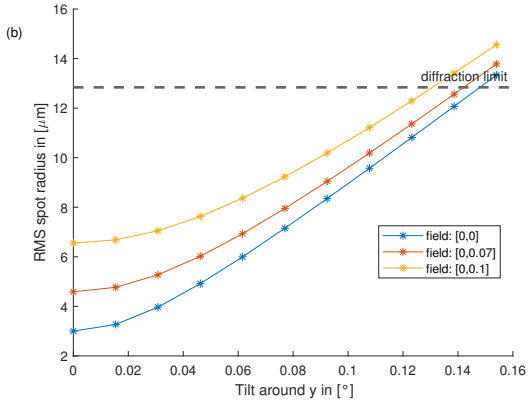

Figure 25: RMS spot radius for different fields in dependent of a tilted objective.

4.6 Movement of the second lens

Because the light coming from the objective is assumed as collimated the distance from the lens to it is irrelevant and not covered in the following. Only the distance between the lens and the camera is changed. That means that the focused beam is not imaged anymore, but changes around this position can be detected. That does not state something about the quality of the objective, but is important to determine the overall performance of the system. Also it is necessary to know the shape of the beam to find the focus before the first measurement.
For this movement along the z-axis the PSF is identical for x- and y-direction and symmetric around the z-direction (Fig. 26). Moving away from the focus will cause a blur of the image, so the first order peak will decrease while the second order one will increase until they reach a similar irradiance value. This is only the case for a system that is far away from the diffraction limit and can't be observed here. The Strehl ratio (Fig. 27a) and the FWHM (Fig 27b) confirm this behavior and also give a range of 1.09 mm for a diffraction-limited system. The minimal spot size, so the beam focused onto the camera,

can be found at a distance of 748.39 mm.This is within the limits of the given focal length of the lens ((750.0 ± 7.5) mm).

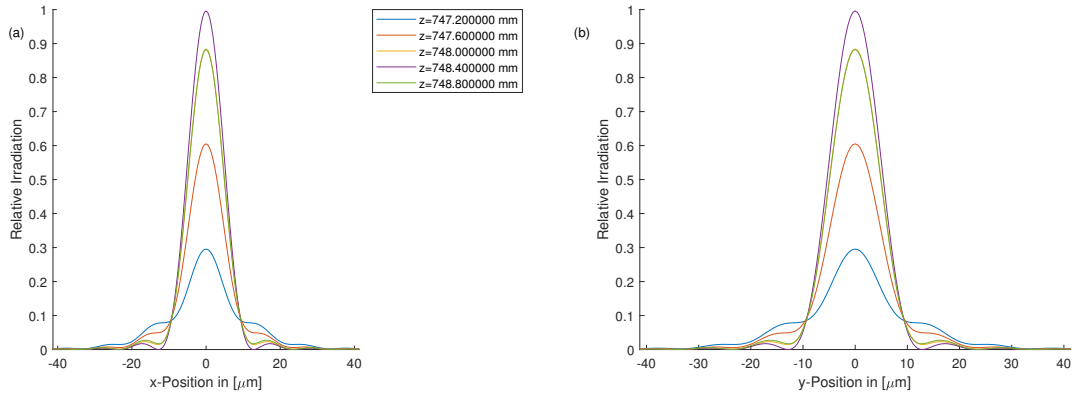

Figure 26: Simulated 1d-PSF in (a) x- and (b) y-direction for a displacement of the focus.

The RMS spot radius states a optimal distance of 748.31 mm between the second lens and the camera and a range of 1.8 mm for a diffraction-limited system. To place the camera in the focus for a field of (0 mm,0.1 mm) the distance needs to be adjusted by −310 µm (Fig. 28).

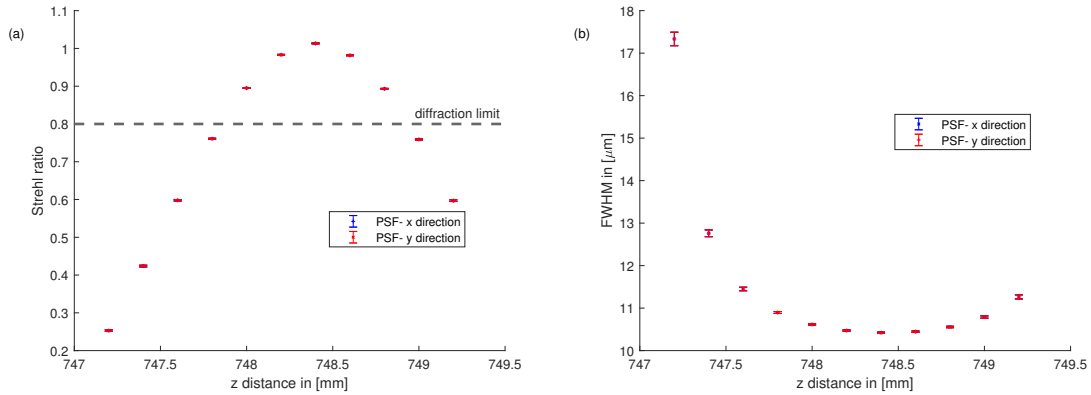

Figure 27: (a) Strehl ratio and (b) FWHM, calculated with eq. 37, dependent on the focal distance. Errorbars are calculated out of the fit error.

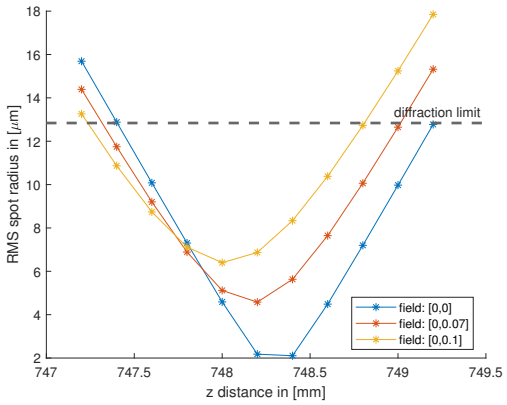

Figure 28: RMS spot radius for different fields in dependent of the distance between second lens and camera.

If the lens is decentered in x- or y-direction the PSF don't shown any change in the Strehl ratio or the FWHM. Only if a part of the beam is not getting focus anymore, because some outer rays don't hit the lens anymore the, the Airy disk will change. This is totally not wanted and not covered here.

4.7 Tilt of the second lens

With a tilted lens, similar to the change of the focal distance, no statement for the objective can be made, but the system as whole is analyzed. Again only the positive rotation around the y-axis is discussed due to the symmetry of the Airy disk and the system.
The PSF shown in Fig 29 is not identical for x- and y-direction, but both are symmetrical around the z-axis. This is surprising, because all other simulations for a tilt show a non symmetric behavior. But the beam hitting the lens is collimated, so every ray has the same angle to the lens, even after a tilt. This explains the symmetry at the z-axis. The collimation is also the reason why the maximum of the PSF in x-direction don't show any movement, the small wiggle is only an error in the simulation. The Strehl ratio (Fig. 30a) also shows the symmetry between both directions. It shows that the diffraction-limited system is obtained until a tilt $> 1.65°$ is reached.

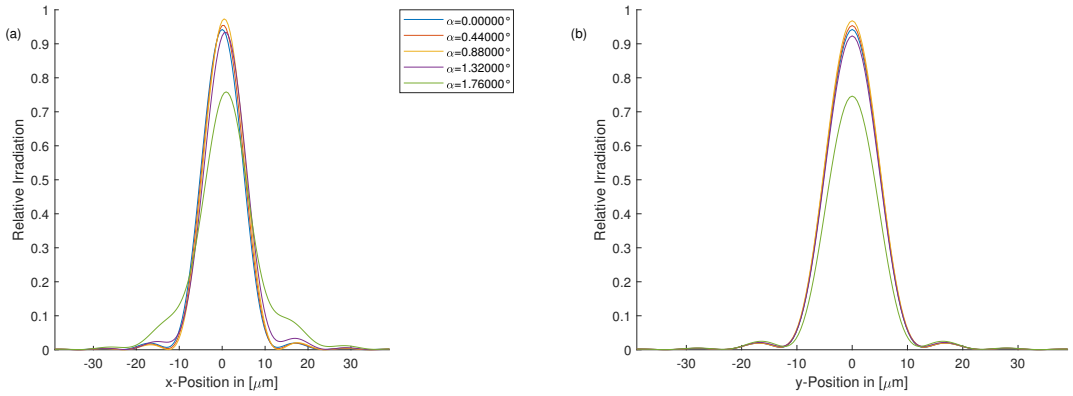

Figure 29: Simulated 1d-PSF in (a) x- and (b) y-direction for a tilt of the lens around the y-direction.

The maximum, this time for both directions, is most likely an effect caused by the fact, that the lens is not specifically designed for a wavelength, so a tilt might compensate for chromatic aberrations. However the FWHM stays constant over the relevant area, as seen

in Fig. 30b. That means that the beam size is actually increasing with a larger tilt.

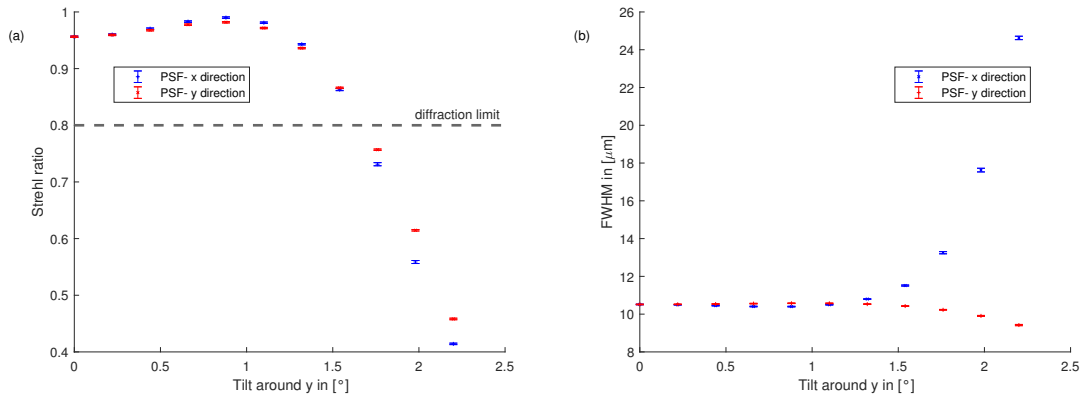

Figure 30: (a) Strehl ratio and (a) FWHM, calculated with eq. 37, dependent on rotation of the second lens. Errorbars are calculated out of the fit error.

The RMS spot radius also shows a minimum at an angle of the lens, but only at a zero field. For a misplacement of the point source this minimum vanishes and only an increase of the spot size can be observed. It can be said that the best result will be acquired if the lens is orthogonal to the z-axis. The range for a diffraction-limited system is 2.15° and 1.79° for a zero field and a decentered light origin respectively.

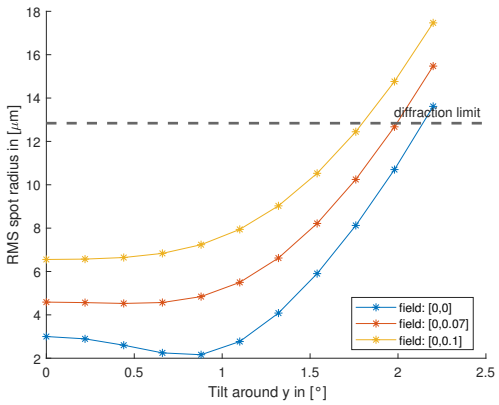

Figure 31: RMS spot radius for different fields in dependent of a tilted second lens.

The camera do not need to be covered here, because it is aligned with no other part inserted into the system. So it will be always at the optimal position and all other parts are placed in dependent of this.

4.8 Compensation of a misplaced objective

As stated in the introduction of this section a change of the distance between window and objective can be compensated by adjusting the focal distance of the second lens. In table 1 the corresponding distances can be found. For a smaller distance between objective and window the focal distance needs to be increased. That means vice versa, that for a larger first distance the focal distance is smaller. The compensations allows for a drastic increase of the range where the whole system is diffraction-limited.

Table 1: Corresponding distances for a compensation of a movement of the objective. The focal distances between the second lens and the camera given in the right column optimize the spot size for the varying distances between the objective and the window.

Distance objective - window [mm]	focal distance [mm]
7.4670	773.36
7.4733	768.84
7.4796	764.36
7.4859	759.92
7.4922	755.52
7.4985	751.15
7.5048	746.82
7.5111	742.52
7.5174	738.26
7.5237	734.04
7.5300	729.85

Without a compensation the obtained range, according to the Maréchal criterion, is 1.62 µm, this range is three times larger ($\sim$ 4.8 µm, Fig. 32a) if the focal distance is changed to minimize the spot size. For the Rayleigh criterion this range increases from 2.47 µm to 6.5 µm as it can be seen in Fig. 32b. The increase here is a bit smaller than for the first criterion. For both methods the optimal position is at 7.495 mm. If the point source is misaligned as well then the optimal position stays the same, but the diffraction-limited range is decreasing and the over all spot size is larger for all distances.

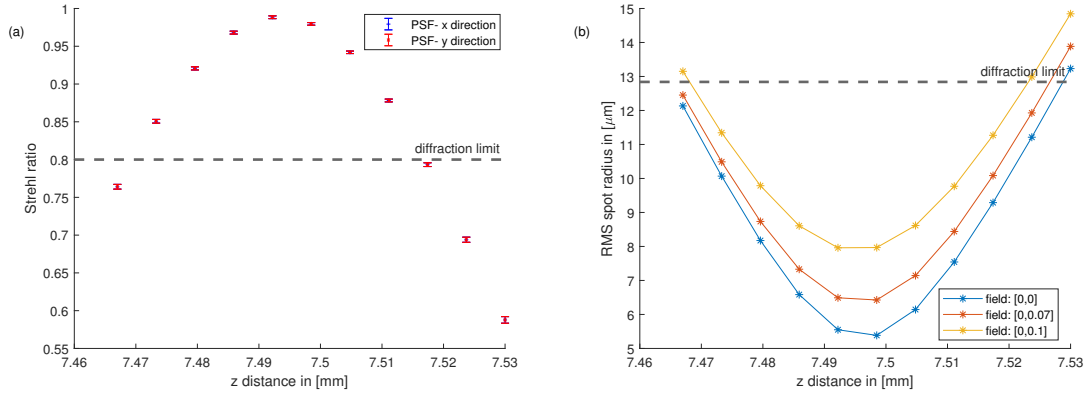

Figure 32: (a) Strehl ratio calculated with eq. 37 and (b) RMS spot radius dependent on the distance between objective and window. The occurring aberrations are compensated by an adjusted focal distance between the second lens and the camera.

4.9 Summary

To have an optimal PSF and determine the boundaries of a diffraction-limited system all optical elements need to be placed and rotated very precisely. The optimal positions and ranges a part can be misaligned to be still diffraction limited can be found in table 2. Most sensitive to misalignments are the distances between the SNOM-fiber end, the window and the objective. Also a critical component is the tilt of the objective. Also all parts of the system should be orthogonal to the beam path, so to the z-axis. If misalignments are compensated by misaligning another part the range, where a diffraction-limited image can be obtained will increase.
There are no simulations for the second wavelength $\lambda = 532$ nm here, because with the detailed one done for $\lambda = 421$ nm it is clear that the general behavior will be the same.

Some values will be slightly different, but the purpose of a diffraction-limited objective will be given in this adjusted area.

Table 2: Optimal position and tilt for the relevant misalignments determined by the simulation for the Machéral and the Rayleigh criterion. The values are displayed as (optimal ± range), where the range gives an approximation how much the part can be misplaced or rotated to still be diffraction limited.

misalignment	Maréchal criterion	Rayleigh criterion
point source - window	$(16.5004 \pm 0.0008)\,\mathrm{mm}$	$(16.501 \pm 0.002)\,\mathrm{mm}$
tilted window	$(0.000 \pm 0.005)^\circ$	$(0.00 \pm 0.02)^\circ$
window - objective	$(7.5033 \pm 0.0008)\,\mathrm{mm}$	$(7.6 \pm 1.3)\,\mathrm{mm}$
decentered objective	$(0.00 \pm 0.05)\,\mathrm{mm}$	$(0.0 \pm 0.2)\,\mathrm{mm}$
tilted objective	$(0.00 \pm 0.13)^\circ$	$(0.00 \pm 0.15)^\circ$
lens - camera	$(748.4 \pm 1.1)\,\mathrm{mm}$	$(748.4 \pm 1.8)\,\mathrm{mm}$
tilted lens	$(0.0 \pm 1.7)^\circ$	$(0.0 \pm 2.2)^\circ$

5 Characterization of the objective

In this section it will be shown that it is possible to image the Airy disk and test its behavior under misalignments with this setup. To do so qualitative images around the focus, taken after every alignment step, are analyzed and discussed. This will not describe a diffraction-limited system, but showcase the possibilities with this setup. With further measurements then the range of the objective to be diffraction-limited can be determined, possible problems identified and the optimal positions found. All of this then should lead into a statement if the objective is capable to be used in the actual experiment and is able to image the cloud of atoms diffraction limited.

5.1 The base image

To have an idea how the beam profile is shaped and to get a comparison for a completed first setup step an image of the diverging light coming directly out of the fiber is taken and fitted with the Gaussian function from eq. 37. Looking at Fig. 33b a few things can be noticed. The alignment is clearly not optimal. The relative irradiance is not the same for the x- and y-direction and in the y-direction an asymmetry is visible. According to the simulations, even if this particular case is not discussed there, both observations together indicate that there is a tilt around the x-direction. Because the camera is realigned after the objective is inserted and the beam path is also controlled with the mirror, so not fixed at this point, this tilt will vanish then. Another problem is the Gaussian fit. If the intensity of the second order peak and of the first minimum is too high, the fit will result with a larger FWHM. This can be avoided by using a lower exposure time so the second order ring is not imaged.

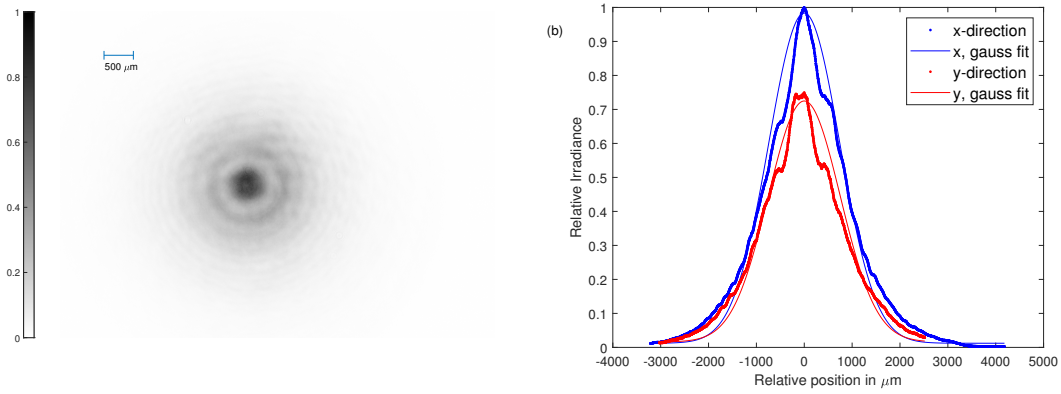

Figure 33: (a) Image and (b) profile of the diverging beam out of the fiber. All irradiations and positions are scaled to the maximum of the data and fitted with a Gaussian function.

5.2 Illumination with a 2 µm diameter fiber

Some first images of the profile from the Airy disk with light going through the objective are shown in Fig. 34a and 34b. The system with all optical elements in place is illuminated by the bare fiber. The images are taken around the focus, by adjusting the distance between second lens and camera, to determine it. Also by this observation possible tilts and misplacements can be detected and corrected. An arbitrary start position is chosen and will give a qualitative reference point.
The symmetry now is given again, which means the tilt is removed. However the difference in the maximum indicates that one part, most likely the objective, is decentered.

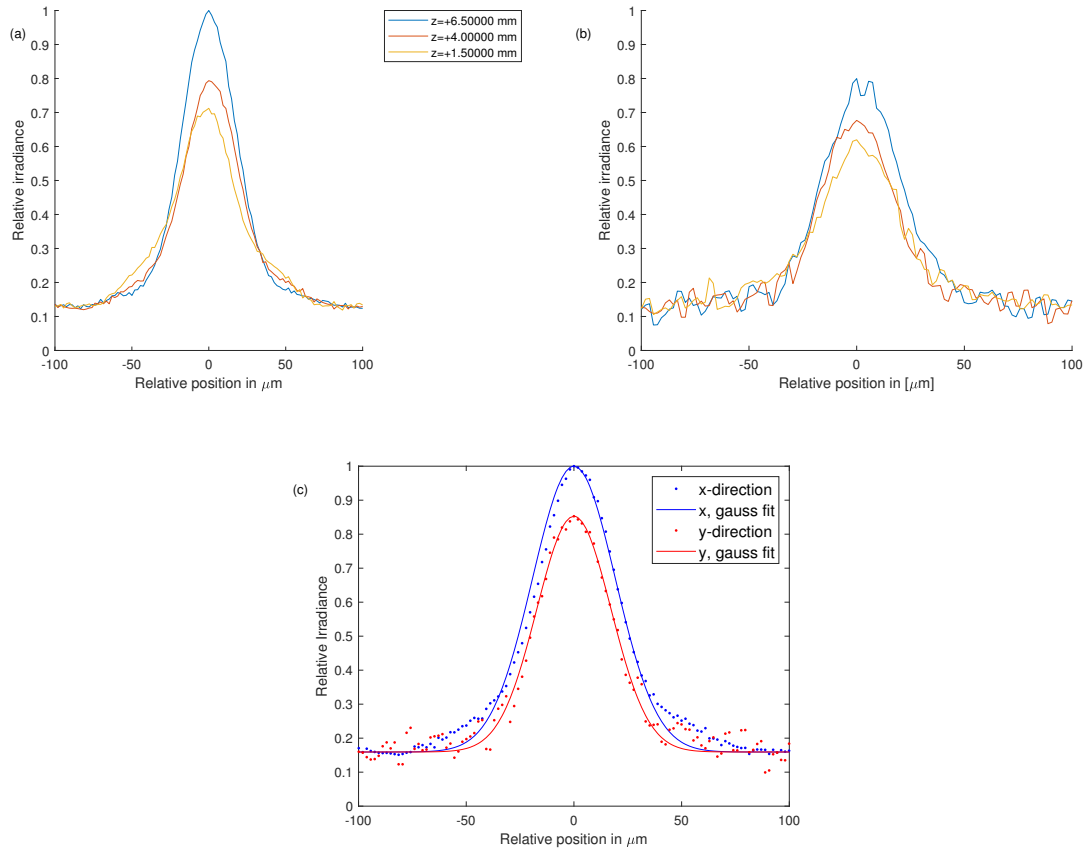

Figure 34: Image data around the focus spot for the (a) x- and (b)y- direction. For a better visibility only a few measurements are displayed. The z-value gives a relative position to an arbitrary chosen start point to image the behavior at the focus. Irradiance and position of all data is are relative to the maximum. (c) shows the Gaussian approximation compared to one set of data.

A small vibration occurs for the x-direction, causing a movement of the maximum. For most measurements this can be ignored and will have no effect on the result. But to determine the impact to the position of the maximum for a tilted optical element, this is a problem. A possible solution is to take multiple images for a specific set of parameters and average them to minimize the effect. But this is not tested and may not be accurate enough.

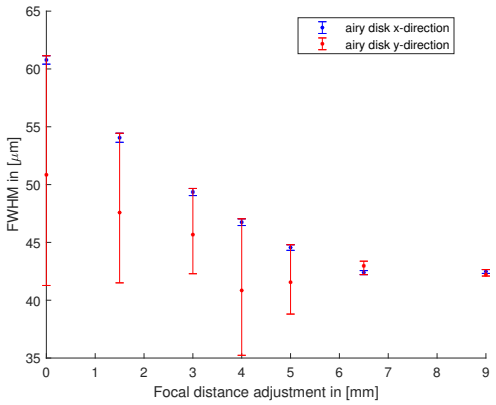

Figure 35: FWHM of the 1d-approximated Airy disk dependent on the adjustment from an arbitrary starting focal distance.

With a low intensity the Gaussian function is now a valid assumption for a fit function as seen in Fig. 34c. That verified, looking at the FWHM (Fig. 35) a possible minimum in the spot size can be found. The scanned distance is not wide enough to determine the exact value, but a range of $4 - 6$ mm where the focus is can be given.
That is a first indicator that the setup is capable of measurements as intended, however to state something about diffraction limit, actual spot radius or aberrations a smaller light source is needed. The next step is to use a small pinhole to shrink the diameter of the light source and get closer to a point-source-like beam.

5.3 Imaging a 1 µm diameter Pinhole

The pinhole diameter is still to large to get any info about the diffraction limit of the objective, but a first analysis can be done with it. A series of images (Fig.36) is taken for a distance of the second lens and the camera around the expected focal length and an, as before, arbitrary starting point. For small relative distances a second order peak can be seen, vanishing as the distance to the focal length increases. The fitted Gaussian functions can be seen in Fig. 37a and 37b.The vibrations are not shown here, to give a better overview and focus on the other parts of the curves. A position near the focal distance means a higher peak for both directions as it is expected. The different peak values for the both directions are again an indicator of a not perfect aligned system.

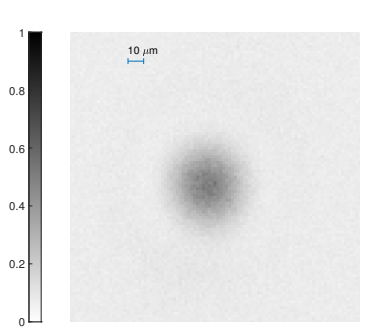

(a) Relative distance $z = 9.5\,\mathrm{mm}$

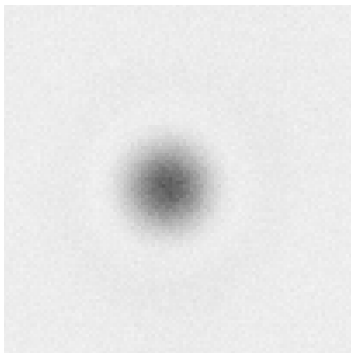

(b) Relative distance $z = 8.0\,\mathrm{mm}$

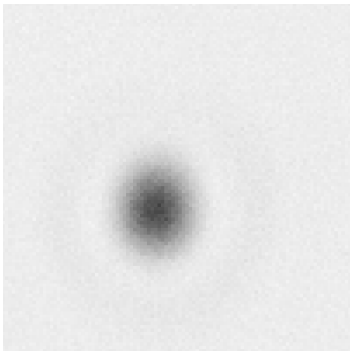

(c) Relative distance $z = 6.0\,\mathrm{mm}$

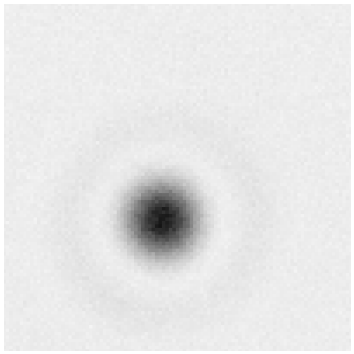

(d) Relative distance $z = 5.0\,\mathrm{mm}$

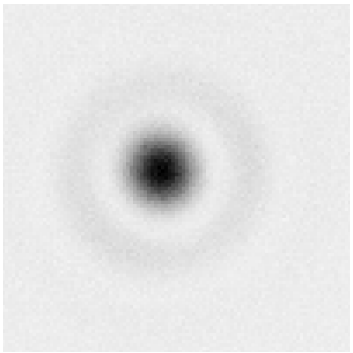

(e) Relative distance $z = 3.0\,\mathrm{mm}$

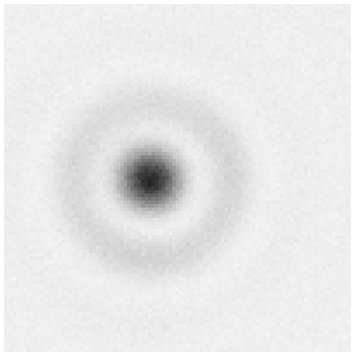

(f) Relative distance $z = 0.0\,\mathrm{mm}$

Figure 36: Images with a pinhole as a point source around the focal distance. For a better visibility the images are displayed as their complement and have a size of 100 by 100 pixels.

With a magnification $m \approx 25$ and a point source diameter of $d = 1\,\mu\text{m}$ the expected spot size is $\sim 25\,\mu\text{m}$. The measured spot size is in the region of 35 to 45 µm. So slightly above the expected value, which is another indicator of a not fully optimized setup.
Figure 37c shows the maximum of the peak in dependence of the distance between lens and camera. It is wrong to speak about a Strehl ratio here because this refers to a system with no aberrations. This can't be guaranteed for the setup in this state. The maximums are scaled to the highest peak, so the most optimal but not necessary perfect one, for better comparability. So an optimal position can be determined and shows that the system has a behavior as expected with a decreasing maximal relative irradiance at distances where the camera is further away from the focus. The FWHM (Fig. 37d) shows a similar tendency for both x- and y-direction. The spot size is increasing if the distance between lens and camera is not correct and has a minimum at the focus. This minimal spot size at the same relative position as for the highest maximum validates the point of the optimal distance. The large errorbars in the y-direction indicate that the Gaussian fit is not a good approximation for these measured data, again a sign that some alignment is far off to the optimal value.

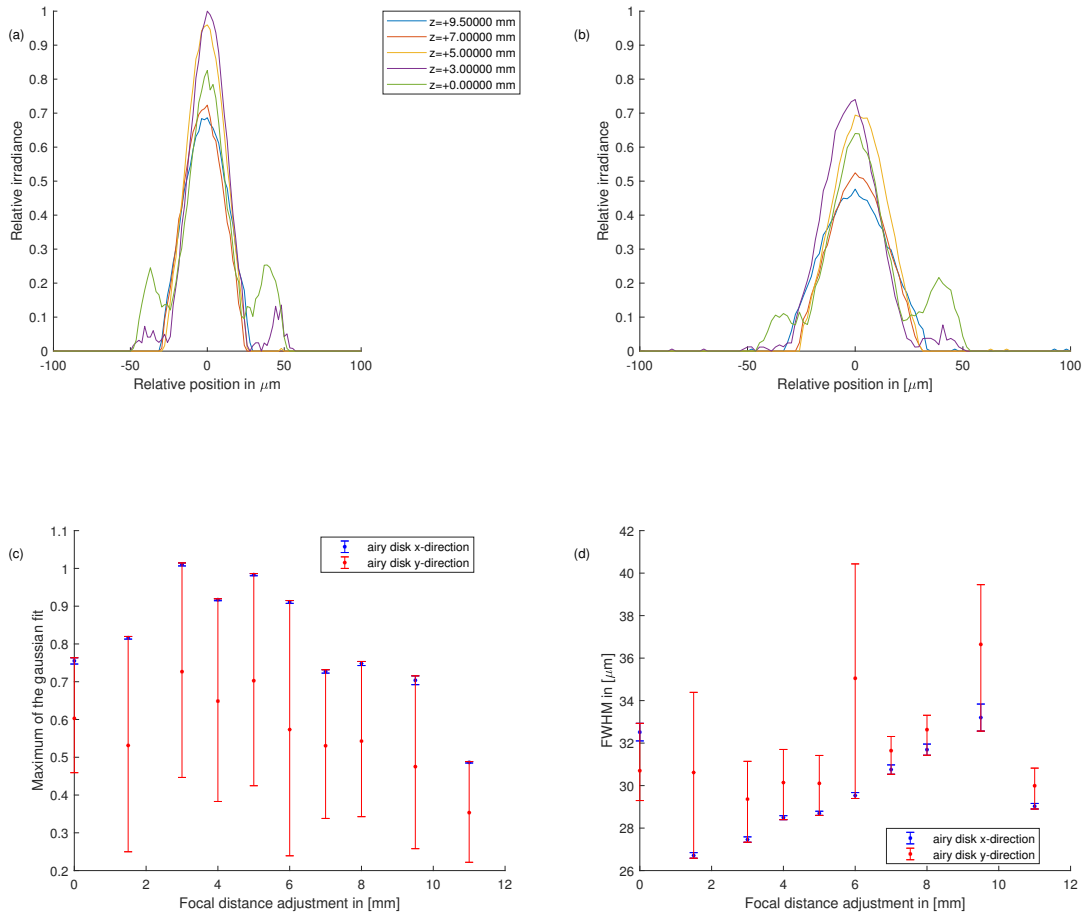

Figure 37: (a) and (b) approximated Airy disk around the focus. The z-value gives a relative position to the starting position. Irradiance and position of the data points are relative to the maximum (c) shows the 'Strehl ratio' and (d) the FWHM from the Gaussian fit with errorbars obtained from the fit parameters.

5.4 First look at the SNOM-fiber

Figure 39 shows a set of images for different distances between the second lens and camera with the full setup in place. A random starting point is chosen, in a way that the theoretical focal length is included. A decrease in the spot size for (a) to (d) can be observed at a subsequent increase. So a minimal spot size, thus the focal distance, can be obtained out of this. The clearly not symmetric shape, with three dots in the center, for (d) and (e) is due to a misalignment of the SNOM-fiber in the last step described in Sec. 3.8. In a next step the mount needs to be completely readjusted because its limit was reached. The images at this point are obviously not Gaussian like functions, so a fit with the so far used eq. 37 will not give the correct values. But it will still show the trend of the focused beam to decrease around the focal distance. For both directions give a position of a minimal spot size can be determined (Fig. 38b). The maxima of the fitted curves, shown in Fig. 38a, also show a optimal position at a similar value. The difference of $\sim 0.1\,\mathrm{mm}$ is due to the large step size between the measurements. Both curves cannot give the exact 'right' position. A difference between the x- and y-direction is a sign of astigmatism, as expected from the system when the light source is not parallel and centered on the optical axis, which is defined by the objective in this case. Also it can not be verified that the beam out of the objective is collimated well enough, because of the low intensity. This can cause additional effects and increases of the spot size as well.
But this shows that in general the setup can be used to calculate the Airy disk of a Gaussian beam and therefore will also be capable to determine the diffraction-limited range of the objective.

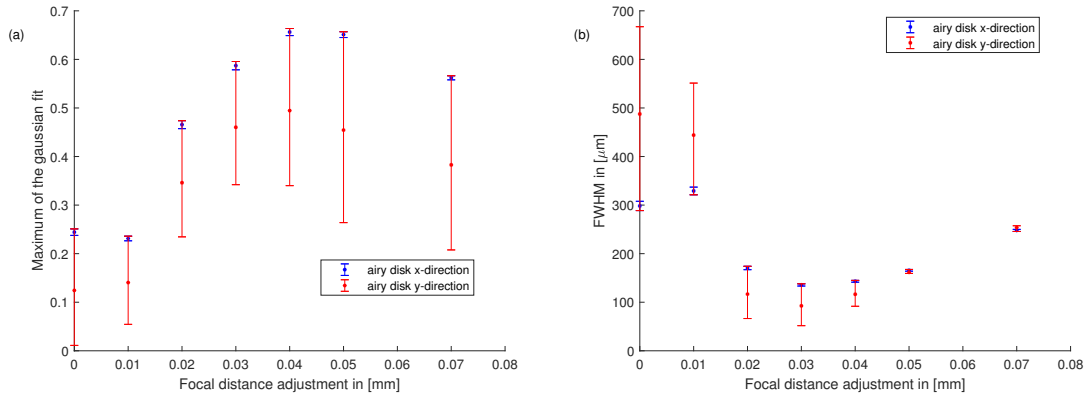

Figure 38: (a) relative maxima and (b) FWHM for the Airy disks from Fig. 39 and a Gaussian fit. The exact values are not relevant here, because of the not solid fit for this misaligned system.

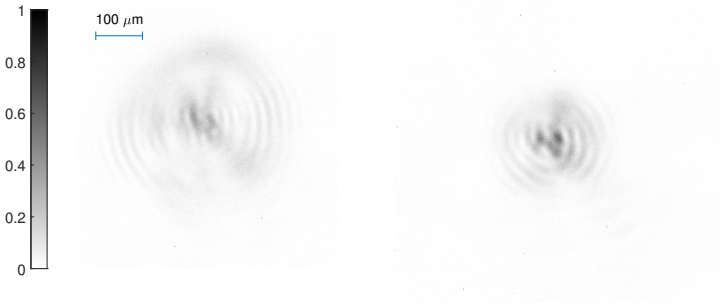

(a) Relative distance $z = 0.07\,\text{mm}$

(b) Relative distance $z = 0.06\,\text{mm}$

(c) Relative distance $z = 0.05\,\text{mm}$

(d) Relative distance $z = 0.04\,\text{mm}$

(e) Relative distance $z = 0.03\,\text{mm}$

(f) Relative distance $z = 0.02\,\text{mm}$

(g) Relative distance $z = 0.00\,\text{mm}$

Figure 39: Images with the SNOM-fiber as point like light source around the focal distance. For a better visibility the images are displayed as their complement and have a size of 300 by 300 pixels.

6 Summary and Outlook

The main goal of this thesis was to give a detailed statement if the objective will be able to work diffraction limited and image structures smaller than 1 µm. This is necessary to image the Dysprosium cloud in the new experimental setup that is currently being built. Also the range where the system is below the diffraction limit under deliberate misalignment, such as decenter, tilt and changed distances between optical elements, should be determined, to give an approximation of how precise the final placement must be. For that purpose a test setup is designed and built. Every part is mounted in a way to control all relevant translations and rotations. A scanning near-field optical microscopy-fiber provides a point-like light source to imitate the experimental conditions. Because the fiber tip aperture is smaller than the structures imaged in the future these test conditions are a stress test for the objective. Another indication of the image quality, thus the limit and quality of the objective, are aberrations. The most present aberration in the test setup is coma, if parts are tilted by a small amount. The theoretical Airy disk is given by the 2d point spread function and misalignments and aberrations can be directly observed by looking at the 1d shape in x- and y- direction. To compare the simulated and the experimental images a Gaussian model is used to calculate the Strehl ratio and the full width at half maximum. The diffraction limit is given by the Strehl and the Rayleigh criterion. Table 2 in Sec. 4.9 gives an overview over the simulated values. The optimal position is determined by the highest value of the Strehl ratio or the lowest spot size radius for both criteria respectively. The range is the calculated area where the system can be changed without exceeding the diffraction limit. The most sensitive parts to be placed are the objective, the window and the SNOM-fiber with their respective distances to each other. The tilt of the objective is also a critical part of the system. Those optical elements must be placed very precisely to achieve a diffraction-limited system. The window has a range for a tilt as well, but in the actual experiment this cannot be adjusted, so this is only a limitation in the test setup.
It was shown that the Airy disk can be observed and with an approximation of a Gaussian function, the peak irradiance and the spot size can be determined. With further data a comparison with the simulated data and a statement to the diffraction limit is possible.
Before further tests can be done, the adjustment of the tilt of the SNOM-fiber needs to be repeated. After that all measurements can be made and compared to the simulations. Also the measurements and simulations for the second wavelength of $\lambda = 532\,\mathrm{nm}$ should be included. With the according fit, then a statement to the quality and limits of the objective can be made. And finally a decision if the objective is suitable for the new experiment can be given. If that statement is positive then it can be inserted and aligned in the actual setup according to the positions and tilts given in the test phase.

References

[1] A. Einstein. Quantentheorie des einatomigen idealen Gases, 1924.

[2] V. K. Lohan. Bose Einstein Condensate as New Form of Matter. International Journal of Physics, Chemistry and Mathematical Fundamentals (www.ijpcmf.com), 15, 03 2016.

[3] A. Griesmaier, J. Werner, S. Hensler, J. Stuhler, and T. Pfau. Bose-einstein condensation of chromium. Physical Review Letters, 94(16), Apr 2005.

[4] M. Schmitt, M. Wenzel, F. Böttcher, I. Ferrier-Barbut, and T. Pfau. Self-bound droplets of a dilute magnetic quantum liquid. Nature, 539(7628), Nov 2016.

[5] F. Böttcher, J.-N. Schmidt, M. Wenzel, J. Hertkorn, M. Guo, Mingyang, T. Langen, and T. Pfau. Transient Supersolid Properties in an Array of Dipolar Quantum Droplets. Physical Review X, 9(1), Mar 2019.

[6] J. Hertkorn, F. Böttcher, M. Guo, J.-N. Schmidt, T. Langen, H.P. Büchler, T. Pfau. Fate of the Amplitude Mode in a Trapped Dipolar Supersolid. Physical Review Letters, 123(19), Nov 2019.

[7] A. Gallemí, S. M. Roccuzzo, S. Stringari, A. Recati. Quantized vortices in dipolar supersolid Bose-Einstein-condensed gases. Physical Review A, 102(2), Aug 2020.

[8] A. Minguzzi, F. Cartarius, G. Morigi. Structural transitions of nearly second order in classical dipolar gases. Physical Review A, 90(5), Nov 2014.

[9] G. De Chiara, J. Boronat, G. E. Astrakharchik, G Morigi. Ground state of low-dimensional dipolar gases: Linear and zigzag chains. Physical Review A, 78(6), Dec 2008.

[10] C. Robens. Testing the Quantumness of Atomic Trajectories. PhD thesis, Rheinische Friedrich-Wilhelms-Universität Bonn, 2016.

[11] F. Kleißler. Assembly and characterization of a high numerical aperture microscope for single atoms. Master's thesis, Rheinische Friedrich-Wilhelms-Universität Bonn, 2014.

[12] W. Demtröder. Experimentalphysik 2 Elektriziät und Optik. Springer Spektrum, 7. edition, 2017.

[13] O. B. Wright A. A. Maznev. Upholding the diffraction limit in the focusing of light and sound. Wave motion, Jan 2017.

[14] D. Meschede. Gerthsen Physik. Springer-Lehrbuch, 2010.

[15] D. Meschede. Optik, Licht und Laser. Vieweg+Teubner, Wiesbaden, 2008.

[16] J. W. Goodman. Introduction to Fourier Optics. Robers and Company, Englewood, Colorado, 3. edition, 2005.

[17] I. Reis. Hochauflösendes Abbildungssystem für ultrakalte Atome. Bachelor's thesis, University of Stuttgart, 2014.

[18] D. G. Smith. Field Guide to Physical Optics. SPIE, 2013.

[19] f/# (lens iris/aperture setting). `https://www.edmundoptics.de/knowledge-center/application-notes/imaging/lens-iris-aperture-setting/`. accessed: 12.10.2020.

[20] M. Gu. Advanced Optical Imaging Theory. Springer Berlin Heidelberg, Berlin, Heidelberg, 2000.

[21] X. Zhang, T. Kashti, D. Kella, T. Frank, D. Shaked, R. Ulichney, M. Fischer, and J. P. Allebach. Measuring the modulation transfer function of image capture devices: what do the numbers really mean?, 2012.

[22] R. A. Schowengerdt. Chapter 3 - sensor models. In Remote Sensing (Third Edition), pages 75 – XIV. Academic Press, Burlington, 2007.

[23] C. Kierans. Testing of a microscope for site-resolved imaging of atoms in optical lattice. Master's thesis, University of Toronto, 2012.

[24] J. Wyant and K. Creath. Basic wavefront aberration theory for optical metrology. Appl Optics Optical Eng, 11, 01 1992.

[25] D. and Z. Malacara. Handbook of optical design. CRC press, 2. edition, 2003.

[26] T. Maier. Interactions in a Quantum Gas of Dysprosium Atoms. PhD thesis, University of Stuttgart, 2015.

[27] R. E. Thomson and W. J. Emery. Data analysis methods in physical oceanography (third edition), 2014.

[28] Zemax, optical design program, users's manual. `https://neurophysics.ucsd.edu/Manuals/Zemax/ZemaxManual.pdf`. accessed: 01.10.2020.

[29] Understanding gamma correction. `https://www.cambridgeincolour.com/tutorials/gamma-correction.htm`. accessed: 01.10.2020.

[30] D. Stack. Optical characteristics of a tilted spherical lens. `ultracold.physics.sunysb.edu/Courses/PHY582-08.Fall/talks/Stack%202008-I.pdf`, year = 2008, note = accessed: 14.10.2020.